AIMS Materials Science, 5(6): 1141–1183.
DOI: 10.3934/matersci.2018.6.1141
Received: 23 September 2018
Accepted: 12 November 2018
Published: 19 November 2018

http://www.aimspress.com/journal/Materials

Review

Nanoporous metals processed by dealloying and their applications

Yong X. Gan[1,*], Yongping Zhang[2] and Jeremy B. Gan[3]

[1] Department of Mechanical Engineering, California State Polytechnic University Pomona, 3801 W Temple Avenue, Pomona, CA 91768, USA
[2] Department of Civil Engineering, California State Polytechnic University Pomona, 3801 W Temple Avenue, Pomona, CA 91768, USA
[3] Diamond Bar High School, 21400 Pathfinder Rd, Diamond Bar, CA 91765, USA

*** Correspondence:** Email: yxgan@cpp.edu; Tel: +19098682388.

Abstract: Porous metals and alloys have many important characteristics such as light weight, high surface area, good electrical conductivity, and enhanced surface plasmonics. They have found many applications in chemical and biomedical engineering fields. This review deals with various dealloying techniques for making nanoporous metals, alloys, and composite materials. Typical dealloying processes and their recent development are introduced. The dealloying techniques include chemical etching, electrochemical leaching, high temperature element removal, thermic reduction, Galvanic replacement, template approach, physical vacuum processing, magnetic field induced processing, plasma reaction etc. Although various noble porous metals such as Pt, Pd, Au, and Ru were extensively studied earlier for applications in catalysis and energy storage/conversions, other porous metallic alloys are under investigations for the removal of pollutants, energy absorbing, filtration of metal ions, organic dyes, and microbial organisms. Advances in processing nanoporous particles, nanosheets, and porous fibers will be discussed. The applications of recently developed nanoporous metals are presented as well.

Keywords: porous metals and alloys; dealloying; nanostructure; manufacturing processes; energy storage; sensing; catalysis

1. Introduction

Porous materials are new engineered materials with high specific surface [1], low density, satisfactory energy absorbing capability [2,3], and high structure stability [4]. In addition, porous

metals have unique mechanical property [5]. Li et al. [2] prepared a nanoporous Co by chemical dealloying Co–Al alloy to generate the pore size in the range from 0.5 to 1.2 nm. The porous Co was then coated with a carbon layer with a thickness of ranging from 1.8 to 4.9 nm. The porous Co@C showed an improved microwave absorption capability due to the magnetic loss caused by the Co core and the dielectric loss of the carbon coating. Dealloyed porous metallic materials have found key roles for electrochemical energy conversion and storage because of their tailored structures suitable for rapid reaction kinetics, high electrical conductivities, and high stability. How nanoporous metals formed by dealloying can meet all of these requirements was discussed in [4]. The characteristics of dealloyed materials related to their functions in energy devices were revealed as well. Nanoporous metal electrodes for applications in fuel cells, supercapacitors, and batteries were presented. In addition, some insights into selection and design criteria for meeting the diverse needs of energy conversion and storage were provided. For nanosensors and actuators, the mechanical responses of the materials used are very important for the sensitivity and lifetime of the devices. Jin, Weissmüller, and Farkas [5] studied the mechanical property of nanoporous metals made by dealloying. The network architectures of dealloyed metals contain nanoscale struts and ligaments. Such a structural feature enhances the mechanical performance for their applications as functional or lightweight high-strength materials in sensing and actuating devices.

Although nanostructured porous materials based on noble metals are extensively used for electrochemical catalysis, energy storage and conversions [6], less noble elements such as silicon and copper, have been made into porous form for various functional applications [7]. A composite porous wick was made by dealloying copper–zinc alloys in NaOH for heat transfer management [8]. Porous silver has been studied for the ethanol fuel cell application [9]. A noble metal may be alloyed with a less noble one, for example: Au with Ni, to form a porous structure for energy conversion [10]. There are many ways to prepare porous metals or alloys [11–13]. Zhang et al. [11] used the spark plasma sintering to obtain nano- to submicro-porous TiMo foams. A solution dealloying method was used to make porous materials for biodegradable implants with the required initial bone mesenchymal stem cell adhesion [12]. In addition, a vacuum dealloying approach was applied for porous stainless steel processing [13]. Typical dealloying techniques can be divided into chemical dealloying, electrochemical dealloying, high temperature method, physical vacuum dealloying, template sacrificial dealloying, plasma reaction, magnetic field enhanced approach, phase separation dealloying, and Galvanic replacement. These methods will be described in next section.

The structure of this paper can be divided into five parts. The first part will be on the dealloying technology. Various methods associated with dealloying processes will be introduced. Typical nanoporous metals made by the dealloying technology will be presented. Following that, the structure and morphology of nanoporous metals, alloys, and composites will be discussed in the second part. In the third part, the properties of the nanoporous materials made by dealloying will be discussed. The fourth part of this review deals with the applications of the nanoporous materials with the emphasis on energy production, storage, and conversions. Finally, research trends and concluding remarks are drawn.

2. Dealloying processing and manufacturing techniques

In this paper, typical dealloying techniques used to generate nanoporus structures will be reviewed. These include chemical dealloying, electrochemical dealloying, high temperature method,

physical vacuum dealloying, template sacrificial dealloying, plasma reaction, magnetic field enhanced approach, phase separation dealloying, and Galvanic replacement. More details in these methods are described as below.

2.1. Chemical dealloying

Chemical dealloying refers to free corrosion or selective leaching of one or more elements from precursor alloys. Bicontinuous structures form due to the removal of the less noble elements in general cases. In [14], a strong acid, nitric acid, was used to selectively remove copper element from gold copper thin films. The Au–Cu thin films were dealloyed in concentrated nitric acid solution in the temperature range from 5 to 35 ℃. The removal of Cu initiated in the interior grain regions. The gold ligaments or void networks started formation at grain boundaries.

Depending on the concentration of nitric acid used in the dealloying process, the chemical reactions are different. In concentrated nitric acid, the dealloying of copper follows the chemical reaction:

$$Cu + 4HNO_3 \rightarrow Cu(NO_3)_2 + 2NO_2 \uparrow + 2H_2O \quad (1)$$

In diluted nitric acid, copper reacts with the acid according to following formula:

$$3Cu + 8HNO_3 \rightarrow 3Cu(NO_3)_2 + 2NO \uparrow + 4H_2O \quad (2)$$

In addition to use strong acid as the etchant for selective leaching, alkaline solutions are also effective to remove elements from precursor alloys. For example, to generate a nanoporous Pt, a 20 wt% NaOH aqueous solution was used to partially etch Al away from an Al–Pt alloy ribbon with the composition of $Al_{85}Pt_{15}$. A two-step etching using different etchants was also performed on the melt-spun $Al_{85}Pt_{15}$ and $Al_{85}Pt_8Ce_7$ alloys. The related chemical reactions for Al removal can be described as:

$$2Al + 2NaOH + 2H_2O \rightarrow 2NaAlO_2 + 3H_2 \uparrow \quad (3)$$

$$2Al + 2NaOH + 6H_2O \rightarrow 2NaAl(OH)_4 + 3H_2 \uparrow \quad (4)$$

For the Ce added alloy, the first step of dealloying using the NaOH etchant removes the Al. The second step of dealloying using nitric acid as the etchant removes Ce and Ce_2O_3 nanorods which were generated in the first stage of dealloying [15]. The process follows the following reactions.

In the first step of dealloying, Ce reacts with NaOH to form cerium hydroxide, i.e.,

$$Ce + 3NaOH \rightarrow 3Na^+ + Ce(OH)_3 \downarrow \quad (5)$$

$$Ce + 4NaOH \rightarrow 4Na^+ + Ce(OH)_4 \downarrow \quad (6)$$

The solubility product constant, K_{sp} for $Ce(OH)_3$ is about 6.0×10^{-22}. This value for $Ce(OH)_4$ is 1.98×10^{-5}. The cerium hydroxide precipitates, $Ce(OH)_3$ and $Ce(OH)_4$, convert to cerium oxides gradually following the equations below.

$$2Ce(OH)_3 \rightarrow Ce_2O_3 \downarrow + 3H_2O \quad (7)$$

$$Ce(OH)_4 \rightarrow CeO_2 \downarrow + 2H_2O \quad (8)$$

Chemical dealloying by 0.1 M hydrochloric acid (HCl) was carried out on a Mn–Cu–Ni alloy to prepare nanoporous copper and nanoporous copper–nickel [16]. When put the Mn–Cu–Ni into HCl, manganese reacts with HCl to generate hydrogen gas and produce manganese(II) chloride as described by the following equation.

$$Mn + 2HCl \rightarrow MnCl_2 + H_2 \uparrow \quad (9)$$

A three-dimensional bicontinuous porous structure with nanoscale ligaments and pores with a pore size of less than 50 nm was obtained. It was found that increasing the nickel content in the precursor alloy could reduce the pore size. Because Ni had a lower surface diffusivity than that of Cu, it slowed down the diffusion and rearrangement of Cu atoms during the dealloying process. It was also observed that the heat treatment at elevated temperatures of 300 ℃, 450 ℃, and 600 ℃ led to the larger ligaments in both nanoporous copper and nanoporous nickel [16].

In the work performed by Liu et al. [17], an $Al_{65}Cu_{23}Fe_{12}$ quasicrystal precursor alloy ribbon was chemically dealloyed in 2 M NaOH to remove Al. The resulted composite product, Fe_3O_4/CuO/Cu, contains bicontinuous ligaments and nanopore channels. This composite has the combined advantages of the high reversible capacity of Fe_3O_4/CuO and the excellent conductive behavior of Cu for lithium ion batteries. The 3D ligament-pore structure is effective in reducing the volume changes during the charge and discharge cycling. The surface of the nanoporous Fe_3O_4/CuO/Cu can be further modified by aminopropyltrimethoxysilane (APS) so that the oxidized graphene sheets can attached to the nanoporous structure [18].

Chauvin et al. [19] studied the dealloying process of silver–aluminum (Ag–Al) thin films in 2 wt% hydrochloric acid. The films were deposited by a DC co-sputtering process of silver and aluminum targets in a confocal geometry using pure argon plasma. Through the change of the deposition parameters such as the electrical powers applied to the targets and the deposition temperature, films with various compositions and morphologies were obtained. The dealloying was able to leach aluminum and generate a nanoporous skeleton of silver. The dealloying reaction rate was found higher for those films with lower silver content. The initial morphology of the Ag–Al films could also influence the aluminum etching kinetics. The rate of leaching was larger when the size of the columns forming the Ag–Al films was smaller.

2.2. Electrochemical dealloying

Electrochemical dealloying is also called galvanostatic or potentiostatic dealloying. It is a controlled corrosion approach. It can be defined as the process in which selective electrochemical dissolution of elements from the based alloys occurs. Sun and Balk [20] reported electrochemical dealloying Au–Ag in concentrated nitric acid. Nanoporous gold formation without volume change or significant cracking was obtained. The method is suitable for fabricating millimeter-scale samples. The nanoscale, interconnected sponge-like structure is sensitive to a focused ion beam (FIB). The exposure to FIB caused immediate and extensive cracking of the nanoporous gold. In addition, FIB also caused the ligament coarsening at the surface of the nanoporous bulk gold material. Nanoporous platinum was successfully prepared from a Cu–Pt alloy plate by electrochemical dealloying [21]. The anodic potential led to the electrochemical dissolution of copper for the Cu–Pt alloy.

Wang et al. [22] prepared an iron-based surface porous network by electrochemical dealloying melt-spun Fe–Si alloy ribbons in 0.6 M perchloric acid. The initial cellular structure prepared by the

melt spinning technique allows the selective electrochemical dissolution of Fe–Si from the alloy ribbons because of the inhomogeneous composition of the center and edge of the cells. The whole electrochemical dissolution process consists of two stages and the entire duration is less than one minute. In the first stage, the surface of the ribbon gradually became flat and the grain structure was revealed. Pores also initiated in this stage as shown in Figure 1a. The lower part of the inset image in Figure 1a reveals the grain boundaries. The upper section shows the porous feature. In the second stage, the pores spread throughout the surface of the ribbon. The average size of pores is about 310 nm and the average size of the ligament is 150 nm as shown in Figure 1b. The associated dissolution mechanism has been proposed. The method is applicable for preparing surface porous materials via selective electrochemical dissolution of cellular structures.

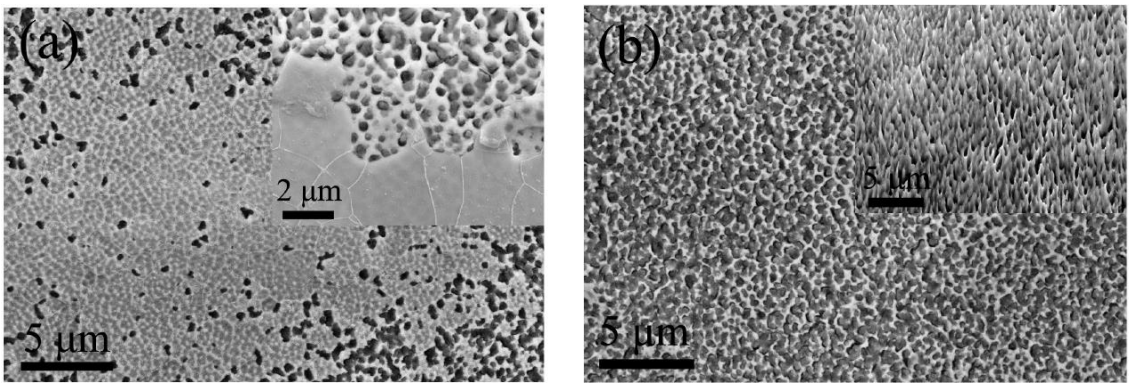

Figure 1. Images showing the electrochemical dealloyed Fe–Si: (a) first stage, (b) second stage [22]. Reprinted (adapted) with permission from Ref. [22].

In the paper published by Paschalidou et al. [23], electrochemical dealloying of an alloy with the composition of $Au_{40}Cu_{28}Pd_5Ag_7Si_{20}$ in 1.0 M HNO_3 was shown. Porous microstructures were obtained from both fully amorphous ribbons and ribbons containing crystals in the amorphous matrix. Dalloying was performed in the aqueous nitric solution at 70 ℃ de-aerated with Ar gas. The dealloying potential was kept at 1.1 V vs Ag/AgCl reference using a Pt grid cylinder as a counter electrode. The dealloying current density was around 1 mA/cm^2. This anodic current allowed the dissolution of most of the less noble elements to form nanoporous gold. Cu and Si were completely removed, while traces of Pd and Ag at 0.5–0.7% were found.

Electrochemical dealloying in neutral solution to make a surface-porous Mg–Al eutectic alloy was reported [24]. The dealloying was carried out at room temperature in a 0.6 M NaCl solution by controlling the applied potential and processing time. Selective dissolution occurred at the surface of the precursor $Mg_{70.5}Al_{29.5}$ eutectic alloy. The surface-pores formed by the selective dissolution of the alpha-Mg phase. The porous layer framework was composed of the remaining $Mg_{17}Al_{12}$ phase. It is possible to control the size of the porous layer by varying the synthesis parameters.

2.3. High temperature dealloying

High temperature dealloying refers to the selective element removal from alloys at elevated temperatures. High temperature dealloying processes are typically accompanied by liquid metal

reactions, solid metal reactions, and/or metal vapor reactions to selectively remove elements from base alloys. The high temperature liquid metal dealloying method has the flexibility in selecting chemical composition of a desired porous material together with unique tunable microstructure. The high temperature liquid metal dealloying has recently been demonstrated as a powerful variation of dealloying. This process uses a melt to carry out selective removal of an element or elements. The melt as a corrosion medium replaces the electrolyte or solution in traditional electrochemical or chemical dealloying. It is reported in [25] that both electrolytes/solutions and molten metals are suitable for dealloying as corrosion media. But they can generate different morphologies. Comparative studies on the microscale physics and chemistry controlling microstructural evolution in electrochemical and liquid metal dealloying showed that the core phenomenology of porosity evolution: a competition between dissolution and interface diffusion, was similar in both dealloying processes. Okulov et al. [26] prepared open-pore Ti–Zr alloy by liquid metal dealloying. In molten magnesium, Ti–Zr–Cu alloys became open porous Ti_xZr_{100-x} alloys with varied chemical compositions and microstructural characteristics. The effects of the processing conditions and the precursor alloys' chemical composition on the microstructure of the porous Ti_xZr_{100-x} as well as their mechanical behavior were studied. The porous Ti–Zr shows a fairly high strength of 480 MPa. Its stiffness ranges from 3.2 to 15.1 GPa. In addition to magnesium, silver is also used for high temperature liquid dealloying. In a silver bath, the copper element in $(Ni_{90}Cr_{10})_{60}Cu_{40}$ precursor alloy diffused into silver. An anisotropic nanoporous NiCr and NiCr–Ag composites were obtained [27]. The resulting microstructure is bi-continuous. A final etching step may be used to removes the Ag solid-state solution phase.

The high temperature dealloying method was used to make tantalum foam with high porosity and wide pore size distribution as reported in [28]. The raw materials: Ta, Ti, and Mg powders, were compacted at ambient temperatures. Then dealloying in vacuum was performed to remove magnesium at a high temperature of 1500 ℃. It must be noted that the boiling point of magnesium is 1090 ℃. During the high temperature dealloying process, it was found that the magnesium diffused from the middle to the surface of the precursor alloys, leaving open spaces surrounded by the Ta–Ti metallic scaffolds. Two porous alloys were made with the compositions of Ta–20 wt% Ti and Ta–30 wt% Ti. Their melting temperatures are as high as 2400 ℃ and 2200 ℃, respectively.

Solid metal dealloying at elevated temperatures can generate finer pores than the liquid metal dealloying approach as found by Wada et al. [29]. A (CrFe)–Ni and Mg diffusion couple was used for the solid metal dealloying study. The polished CrFe–Ni alloy and magnesium were pressed together and firmly bolted with stainless steel screws. The diffusion couple was put into a sealed quartz tube at the vacuum level of 10^{-3} torr. Ni selectively reacted with Mg to form a solid Ni–Mg phase when the diffusion couple was heated up to the temperature range from 440 to 480 ℃. This Ni–Mg phase can be readily removed by dissolution in 0.5 M nitric acid at room temperatures. The Fe–Cr phase was left behind because of much higher corrosion resistance of the Cr-containing phase. The remaining Fe and Cr formed various morphologies. The nitric etching resulted in the interconnected Fe–Cr alloy with a ligament width below 200 nm, which is about one order of magnitude finer than that obtained for dealloying with Mg melt. The formation of ordered single-crystal nanofilaments at the dealloying front suggests that the microstructure evolved via the interfacial spinodal decomposition and diffusion-coupled growth mechanism.

High temperature dealloying is considered as a practical pathway to nanoporous Ti alloy surfaces. Panagiotopoulos et al. [30] reported the preparation of nanoporous Ti–Sc alloy via the high

temperature spinodal decomposition followed by chemical dissolution of one of the component products of the phase-separation. The based Ti–Sc alloy was made by melt spinning on a single copper roller. Ti–Sc alloys were revealed by chemical etching with a 70% nitric acid (HNO_3) solution. A hydrofluoric acid (HF) solution was used for chemical etching of pure Ti foils for comparison as HNO_3 did not attack pure Ti; titanium exhibits excellent corrosion resistance to HNO_3 at room temperature. The spinodal wavelength of near 100 nm was achieved in the prepared nanoporous Ti–Sc alloy. It is found that the pores are deep. This is meaningful because the pores can be loaded with bioactive compounds such as proteins or antibacterial drugs, which allows the porous Ti–Sc to be useful for medical implant applications.

Open porous TiFe and TiNb alloys with a yield strength of 150 MPa and stiffness ranging from 2.9 to 4.5 GPa were made by the liquid metal dealloying in molten magnesium [31]. Two dealloying temperatures, 1073 K and 1173 K, were used to separate copper from the precursor alloys. Several precursor alloys including $Ti_{26}Nb_4Cu_{70}$, $Ti_{27.0}Nb_{2.4}Cu_{70.6}$, and $Ti_{29.2}Fe_{3.9}Cu_{66.9}$ were investigated. During the high temperature liquid magnesium dealloying, copper formed new phase with magnesium and was removed by the subsequent procedure by soaking in 3 M HNO_3. The chemical composition of the porous Ti–Nb is $Ti_{89.4}Nb_{10.6}$. The porous Ti–Fe has a composition of $Ti_{88.2}Fe_{11.8}$. Traces of Cu may exist in some samples, but Mg metal was not detected in the porous alloys. The porous alloys were made into metal–polymer composites by subjecting the porous metallic alloys to vacuum for 10 min and then placing them in contact with the liquid Bisphenol F epoxy resin. The yield strength of the composites increases to 260 MPa exceeding that of bone while the stiffness remains below 5.2 GPa. The dealloying-based porous alloys and interpenetrating-phase composites have the potential for biomedical implant applications.

A multiple-step liquid metal dealloying method was used to make a hierarchical porous Fe–Cr alloy [32]. The precursor is a casting ingot of Fe–Cr–Ni–Mn alloy. Two molten metal pools were used for the multi-step high temperature dealloying. Mg melt was used first to remove Ni from the precursor due to the immiscibility of magnesium to other elements. The leaching out of Ni generates large sized bi-continuous pores as also shown in [33] for a Fe–Cr–Ni precursor alloy with the composition of $(Fe_{0.8}Cr_{0.2})_{30}Ni_{70}$. Then, molten Bi was used to remove Mn and remaining Mg from the first dealloying step to generate fine pores. The resultant Fe–Cr porous metal has a hierarchical morphology with a bimodal pore distribution. Such a state allows the Fe–Cr porous material to have a higher porosity and specific area than the one-step dealloyed material.

2.4. Physical vacuum dealloying

Physical vacuum dealloying (PVD) is a process by subliming one or more metal components in an alloy to form a porous metal [34–36]. The foundation for the physical vacuum dealloying is believed to be the Kirkendall effect which refers to the motion of the interface between two metals that occurs as a consequence of the difference in diffusion rates of the metal atoms. The temperature of vacuum dealloying is typically lower than the melting point of the precursor alloy for pore formation [34,35]. For example, Sublimation of Zn from Cu–Zn precursor alloys at 500 ℃ under vacuum becomes the predominate mechanism for the physical vacuum dealloying of zinc from brass. The difference in the saturated vapor pressure of each element in the Cu–Zn alloy is critical for establishing the gap in diffusion rates. It was calculated that the saturated vapor pressure ratio p_{Zn}/p_{Cu} is about 2.14×10^{13} at 500 ℃ [35].

Porous copper has been made successfully by physical vacuum dealloying method using Cu–Zn precursor alloys which are $Cu_{30}Zn_{70}$, $Cu_{40}Zn_{60}$, and $Cu_{50}Zn_{50}$ [34]. The porous copper showed a three-dimensional continuous porous structure. The size of the pores ranges from 1 to 5 μm. With the increase of the Zn content in the precursors, the porous copper has a more uniform and ordered structure. Temperature is a critical factor in the physical vacuum dealloying. The pores would fuse and disappear when the temperature was too high. In literature [36], four different temperatures: 450 ℃, 500 ℃, 550 ℃, and 600 ℃ were used for the physical vacuum dealloying of a brass with the composition of $Cu_{30}Zn_{70}$ at a vacuum level of 10 Pa for three hours. 500 ℃ was found to be the optimized condition. Three dimensional continuous pores with the ligament size of 1 to 2 μm were obtained. It is predicted that physical vacuum dealloying could be used to prepare other porous metals besides copper [34].

2.5. Template sacrificial dealloying

Template sacrificial dealloying or simply called template dealloying as described in [37–43] refers to the process of using a template as a substrate to make an alloy first. High temperature annealing or chemical dissolution is used to remove the template material. Then a selective removal of the less noble element from the alloy is performed. In recent work presented by Zhang et al. [37], colloidal polystyrene (PS) microspheres aligned on silicon wafers were used as the templates for making nanoporous gold arrays. It is demonstrated that using the PS template can prepare two-dimensional, highly ordered, large-area nanoporous gold and gold–silver alloy arrays. Briefly, the approach consists of depositing gold on PS spheres followed by high temperature removing the PS spheres. The temperature used was 1000 ℃. After that, a less noble metal, silver was deposited on the gold. Then gold–silver alloys were obtained by annealing at 600 ℃ in a protective atmospheric environment. After being cooled down, the specimens underwent dealloying in nitric acid solution for different time to remove the silver and generate porous Au and/or Au–Ag alloy arrays with different periodic lengths and tunable gold to silver composition ratios. The obtained porous Au–Ag nanoscale spheres are highly porous and have the bicontinuous morphology of hierarchically interconnected ligaments. It was found that with the increasing of the dealloying time, the average size of the nanoporous alloy was slightly decreased. But the width of the ligaments was increased. The periodic length of the nanoporous Au–Ag arrays could be varied by controlling the size of the original PS spheres in the template. The nanoporous Au and Au–Ag arrays were tested as a platform for the surface-enhanced Raman scattering (SERS) detection of 4-aminothiophenol (4-ATP). Since the periodic arrays contain large amount of active spots for detecting, both high sensitivity and repeatability were obtained. As low as 10^{-10} M concentration of 4-ATP could be detected by the porous Au–Ag nano-sphere array sensor.

Modeling, preparation, and characterization of ultralow density metal foams by the template-dealloying approach have been reported [38,42,43]. In the work performed by Yi et al. [38], an analytical-numerical model for hollow metal foams with a two-level hierarchical structure was proposed. A main backbone structure and a secondary nanoporous one are considered in the two-level model. The main backbone is made of a hollow sphere-packing architecture made by removing the PS spherical template as shown in Figure 2, while the secondary nanostructure consists of a bicontinuous nanoporous network representing the nanoscale interactions in the gold shells. In Figure 3, the scanning electron microscopic images of the hierarchical porous gold are shown.

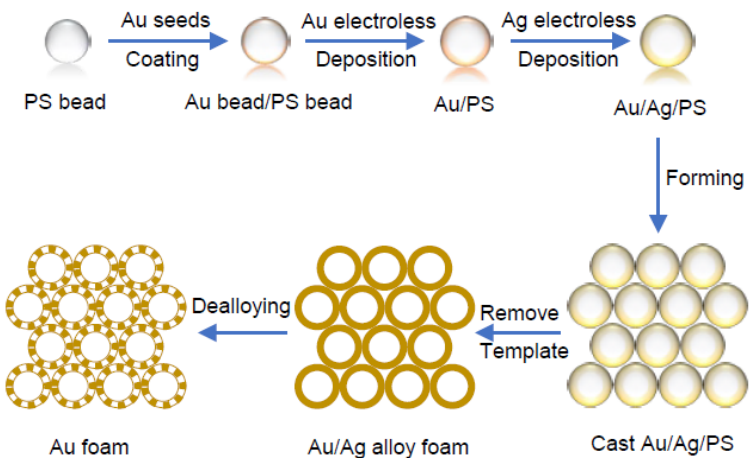

Figure 2. Schematic of the template-dealloying to make porous gold foam [38]. Reprinted (adapted) with permission from Ref. [38].

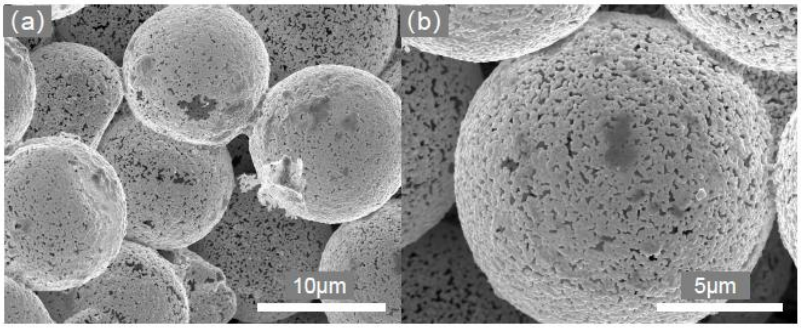

Figure 3. SEM images of the porous gold with a hierarchical structure [38]: (a) the main backbone of a hollow sphere-packing architecture by removing the PS spherical template, (b) the bicontinuous nanoporous gold network in the shells. Reprinted (adapted) with permission from Ref. [38].

The model was found applicable for predicting the stiffness and strength of the template-dealloyed gold foams. Two nanoporous models with different geometries were generated by the Voronoi tessellation. The scaling laws of the mechanical properties were determined as functions of relative density by finite volume simulation. Specifically, the scaling laws were applied to identify the uniaxial compression behavior of metal foams. It is found that the thickness and relative density significantly influence the Young's modulus and yield strength, and vacancy defect determines the foams being self-supported. The present study provides not only new insights into the mechanical behaviors of both nanoporous metals and metal foams, but also a practical guide for their fabrication and application [38].

Li et al. [39] made a series of monolithic porous Au with different pore sizes by the template-dealloying corrosion method. Instead of using PS as the template, they took spherical Cu particles as sacrificial templates. Gold layer was deposited on the copper spheres through electroless plating. A two-step corrosion technique was applied to dissolve the Cu component by $FeCl_3$ and HNO_3, respectively. The microstructure and phase evolution, as well as the effect of the corrosive media, are investigated in this study. As a result, the prepared monolithic porous Au possesses ultra-low density

and a special hollow porous core–shell structure. The density of the corresponding porous structure is as low as 0.37 g/cm^3, which is less than 2% of the density of solid Au [30].

A nanopatterned photoresisist layer can be used as the sacrificial template thorough a lift-off procedure for making porous metals or alloys. For example, porous Au–Ag alloy nanowires were made by such an approach [40]. A nanograted photoresist layer served as a mask for a lift-off process. Laser interference lithography was employed for the nanopatterning of the photoresist layer to create the large-area nanostructured mask. Subsequent evaporation of silver and gold caused the formation of stacked Au/Ag nanoribbons. The stacked nanoribbons were converted into Au–Ag alloy nanowires by the thermal annealing at 800 ℃ for 2 h. Porous Au/Ag nanowires were obtained by etching the alloy nanowires in concentrated nitric acid. A low Au-to-Ag ratio of 1 leads cracks in the dealloyed nanowires. To reduce the internal residual stress generated during the dealloying process, the Au-to-Ag ratio to 3 was found helpful in overcoming the cracking tendency. An array of highly ordered nanoporous gold nanowires was generated. It is suggested that the nanoporous gold nanowire array could be used for sensor and actuator applications [40].

In addition to soft templates, ceramic hard templates are used for template dealloying. The hard ceramic templates may be made of aluminum oxide, silicon oxide, and zirconium oxide. For example, by using silica as a hard template, Luc and Jiao [41] prepared porous metal based compounds. First, a porous silica template was filled with an inorganic precursor (often a metal nitrate salt). During a thermal annealing process, the metal salt was converted into an intermediate phase within the silica pores. Then, the removal of the silica template in either a strong base or a hydrofluoric acid solution produces metal compounds.

2.6. Plasma etching reaction dealloying

Nanoporous materials can be made by selective removal of element(s) through plasma reaction(s). Lee et al. [44] used oxygen plasma to etch carbon from noble metal–carbon thin films with an initial thickness of 500 nm. Nanoporous (np) noble metal thin films with the final thickness of 300 nm containing mesopores (2–50 nm) or macropores (larger than 50 nm) were obtained. First, they deposited the noble metal–carbon thin films on silicon substrates using three different metals targets: Au, Pt, and Ag in argon-methane plasma. The sputter coating generated the 500 nm thick noble metal films. Then O_2 plasma was triggered to selective removing carbon from the surface of the thin films. Carbon atoms diffused from inside the films to the surfaces and were continuously taken away by the O_2 plasma. Consequently, nanoporous metal structures formed. It is reported in more details that by using this method, various nanoporous thin films of Au, Ag, and Pt were successfully fabricated [44].

In addition to remove elements, plasma may also be used to synthesize nanoparticles for the subsequent dealloying. Hydrogen plasma-metal reaction (HPMR) followed by chemical dealloying was reported to make nanoporous Ni particles [45]. After the nickel particles were generated, passivation at room temperature allowed the formation of an oxide layer outside the Ni particles. Such a surface oxidation produced the Ni@NiO nanoparticles with a size of 48 nm. The nickel nanoparticles exhibit a highly porous structure with a pore volume of 0.812 cm^3/g. Hydrogen plasma-metal reaction method was also used to prepare a Ni–Al alloy. The Ni–Al alloy with a composition of $Ni_{45}Al_{55}$ was use for preparing Al_3Ni_2@Al nanoparticles. The dealloying of Al_3Ni_2@Al produced porous Ni@NiO nanoparticles with a size of 36 nm. The pore size was in the

range from 0.7 to 1.6 nm, and the specific surface area reached 69.5 m^2/g. The pore volume of 0.507 cm^3/g was found. The microporous Ni@NiO nanoparticles exhibited an excellent property of microwave absorption in the X-band frequency range. It is believed that the enhanced microwave absorption behavior is due to the micropore architecture. This architecture shows the synergistic effect of the magnetic Ni core and dielectric NiO shell [46].

The hydrogen plasma-metal reaction is not limited to manufacturing nickel based porous materials. Li et al. [47] reported the application of the HPMR method for making Co–Al nanoparticles with a pore size of 45 nm. The nanoparticles display core shell structure with $Al_{13}Co_4$ and CoAl core and aluminum oxide shell (about 2 nm). Under ultrasonic irradiation, nanoporous face centered cubic cobalt nanoparticles were produced successfully by chemical dealloying the Co–Al nanoparticles at room temperature in a sodium hydroxide solution. Ultrasonic irradiation played an important role in the dealloying process. Without the ultrasonic irradiation, CoAl phase could hardly react with the sodium hydroxide solution [47].

2.7. Magnetic field enhanced nanopore formation during dealloying

In magnetic field, the dealloying kinetics can be changed. In recent work, the effect of an external magnetic field on different dealloying stages of the formation of a nanoporous magnetic material was studied [48]. It is found that a low magnetic flux density prolongs the Ni rearrangement. A high magnetic flux density results in the accelerated Ni rearrangement process. Consequently, much finer morphology of nanoporous Ni can be prepared by increasing the external magnetic field strength [48].

2.8. Other methods for nanopore generation

Phase separation can form nanoporous metals as reported in [49]. It is found that the viscoelastic phase separation of colloidal suspensions can be interrupted to form gels either by glass transition or by crystallization. Under a confocal microscope, the transition from a homogeneous phase to different arrested states was observed. The observation also revealed the sponge-like porous crystal structure formation due to the phase separation. In the early stage of phase separation, the nucleation requires a structural reorganization of the liquid phase, called stress-driven ageing. Once the nucleation started, the crystallization followed three different ways: direct crystallization of the liquid phase, the Bergeron process, and Ostwald ripening. Nucleation started inside the reorganized network, but crystals grow past it by direct condensation of the gas phase on their surface, driving liquid evaporation, and producing a network structure different from the original phase separation pattern. Similar crystal-gel states can be found in monatomic and molecular systems as long as the liquid phase generates viscoelastic phase separation and prevents immediate glass transformation.

Galvanic replacement followed by chemical dealloying generated a 3D hierarchical porous platinum [50]. On an aluminum foil, Pt–Cu alloy dendrites were obtained from a fluorinated solution containing Cu^{2+} and Pt^{4+} ions. Due to the fluoride-assisted Galvanic replacement as shown earlier in [51], three-dimensional (3D) porous PtCu dendrites were deposited on the aluminum foil. The aluminum foil can be readily removed by NaOH. Following that, the chemical dealloying in nitric acid to selectively dissolve the less noble metal Cu from the PtCu alloys was performed, which

allowed the formation of the nanoporous Pt. The Galvanic replacement method has also been used to make bimetallic porous sponges and dendritic nanostructures [52,53].

Electrodeposition or electroplating can generate nanoporous structures [54–57]. In [54], electrodeposition of nanoporous nickel from a block co-polymer solution has been demonstrated. The electrodeposited Ni films showed a gradient porosity, with smaller pores and thicker pore walls close to the film's surface. The electrodeposited porous nickel showed a decrease in the Young's modulus, an increase in yield stress and a constant hardness when the maximum applied load during nanoindentation was increased. The decrease in the Young's modulus can be explained by the thickness inhomogeneity of the electrodeposited porous nickel (with an increase in the porosity with depth). The observed increase in the yield stress is due to the decrease in the ligament size. The process for the electrodeposition is also detailed in [54]. In brief, the electrolyte was prepared by mixing the pluronic P123 amphiphilic block copolymer surfactant and aqueous solution of 0.4 M $NiSO_4$, 0.5 M Na_2SO_4, 0.2 M boric acid, and 0.5 g/L saccharine. To prepare the mixture, 4 g of P123 was heated to 60 ℃ and added into the aqueous phase. Then certain amount of ethanol was added into the mixture to assure a ratio of 0.2 g P123 per mL of ethanol. The resulting solution was subjected to vigorous magnetic stirring until it showed a turbid milky appearance. The nanoporous Ni was obtained at room temperature by applying a constant potential of −1.8 V for 1200 s. The concentration of surfactant was set at 8 wt% which is above the critical micelle concentration of P123. A hydrophilic Au substrate provided the aggregation sites for P123, as the surfactant gathers spontaneously at the solid–liquid interface. The surfactant micelle directs the Ni^{2+} ions towards the substrate and acts as a structure-directing agent. The growth of Ni follows a nearly layer-by-layer process, in which the pore size decreases gradually along the vertical direction. This layer-by-layer growth fashion was clearly shown. The first stage of electrodeposition exhibited the largest pore size of 70 nm. As deposition proceeds, a second Ni layer formed on top of the first porous Ni. This second layer had smaller pore size around 10–20 nm.

Electrodeposition is widely used to prepare precursor alloys for dealloying. To make three-dimensional (3D) bicontinuous nanoporous platinum, binary Pt–Ag alloys are electrodeposited on gold substrates [55]. Dealloying was performed following the annealing process. 3D nanoporous platinum-based electrodes were obtained. The morphology, porosity, and chemical compositions were changed by adjusting the electrodeposition parameters and using different plating solution composition. The nanoporous structure showed the pores and ligaments in the 10–30 nm range arranged in a bicontinuous form. The electrodes are actually ternary alloys containing platinum, gold, and a small amount of residual silver that remains after the dealloying.

The electrodeposition process also used for the fabrication of highly porous PtCu alloy anodes. In the fabrication process, Pt and different amounts of a second noble metal (Pd, Ru, and Au) are repeatedly co-deposited with Cu from an aqueous electrolyte, followed by selective dealloying of Cu. Highly porous Pt–Cu alloys with roughness factors ranging from 400 to 4000 can be obtained. In all cases, both noble-metal partners are present on the electrode surface, whereas the majority of copper is likely buried underneath. Compared to Pt–Cu anodes, small additions of Ru (3 at% Ru) lead to significantly enhanced catalytic activity for the electro-oxidation of formic acid and methanol, whereas Au-rich Pt–Cu–Au alloys (75 at% Au) exhibit significantly improved electrocatalytic activity for glucose oxidation [56].

In addition to the electrodeposition approach, the electroless deposition method was used to deposit coatings for the subsequent dealloying. For example, the amorphous Ni–P coatings were

deposited onto Ti substrates by the electroless method. Then, etching in nitric acid with various concentrations was performed [57]. Such coatings were porous. They were tested as the electrodes for supercapacitors. It was found that the dealloying of the Ni–P coatings by acid etching can significantly improve the supercapacitors' performance. The specific capacitance increased 40-fold which is due to the formation of the porous structure and thus the increase of the surface area. Ni was selectively dissolved in the acid solutions to generate nanopores.

3. Structures of dealloyed porous metals

Many researchers have studied the structure development of dealloying in view of the evolution of two-dimensional (2D) and three-dimensional (3D) pores, growth of ligaments, formation of surface pores and solid cores, generation of core–shell architectures, etc. [58]. Especially the hierarchical porous metallic materials have attracted a lot of attentions due to their specific industrial needs. In literature [59], a review on the development of dealloying-enabled hierarchical porous structures was presented.

Temperature induced surface reconstruction and interface structure evolution on ligament of nanoporous copper (NPC) was studied [60]. A copper aluminum alloy with the composition of $Al_{30}Cu_{70}$ was dealloyed in a 5% HCl solution at different temperatures. With the increase of the dealloying temperature, the ligament surface morphology of the NPC changed from smooth to rough. Finally, dispersed single-crystal nanoparticles with significant changes of interface structure from coherence to semi-coherence and to noncoherence were observed. The modification on the surface structure of a nanoporous gold by surface relaxation via electrochemical redox cycling in 0.1 M sulfuric acid has been studied [61]. Just through controlling the scan rates, nanoporous gold with abundant {111} facets or {100} facets can be obtained. At a lower potential scanning rate of 5 mV/s, the nanoporous gold exposes its {111} plane. Increasing the potential scanning rate to 50 mV/s resulted in the {100} plane as the surface layer. The surface energies of different crystallographic planes in gold can be ranked as $\gamma_{(111)} < \gamma_{(100)}$ based on the calculation using a modified embedded-atom method [62]. It is therefore concluded that the surface energy becomes the driving force for the facet evolution and the surface reconstruction during potential cycling. The structure dependence on the scan rate can be explained by the surface relaxation during oxidation and reduction electrochemical reactions. At the low scan rate of 5 mV/s, there is a sufficient time for diffusion controlled surface reconstruction, leading to minimize the surface energy through the formation of the {111} facets. On the contrary, when the scan rate increased to 50 mV/s, the gold atoms at the high-energy sites may not have sufficient time to reach the lowest energy state. Therefore, the formation of {100} facets with a higher surface energy was found. In [63], the hierarchical pore formation and additive manufacturing 3D porous structures are reviewed. The structure design of various nanoporous materials including nanoporous copper in cellulose nanofiber, 3D printed porous Ti, porous Ti–6Al–4V, and porous CoCr was discussed.

Gradient pore size control was introduced in [64]. Basically, a Cu–Mn alloy was dealloyed segment by segment at varied temperatures. The change in the dealloying condition allows the pore size varied. The experiment showed that the pore sizes of the prepared nanoporous copper increased along one direction with the elevated corrosion temperature. Eventually, a 3-D connected network structure with gradient pore size in the dealloyed materials was obtained. Such a segmental

dealloying method can be used to fabricate various other gradient nanoporous materials including those noble metals: Au, Ag, Pd, and Pt.

The thermally and chemically activated pore size evolutions in nanoporous gold were investigated [65]. Surface diffusion has been considered as the major mechanism for the pore coarsening during the thermal annealing and catalytic reaction of converting CO to CO_2. Experimental results were presented to illustrate the surface gold atom diffusion controlled ligament and pore coarsening mechanism. A chemically dealloyed nanoprous gold was made and annealed at 523 K for different time periods including 0.25, 1, and 2 h. It was found that the size of the ligaments in nanoporous gold changes from about 15 nm to 100 nm. Not only the pore size increased a lot, but also the shape of the pore changed from irregular shape to rounded form. Similar pore and ligament coarsening phenomena was observed when the nanoporous sample was kept in CO-containing atmosphere for 0.5, 2, and 4 h at 298 K. The major reason for the structure coarsening is believed from the thermally and chemically activated surface diffusion of the gold atoms. The activation energies for both the thermal and chemical annealing were determined. The data showed that the thermal annealing and catalytic transformation induced coarsening processes exhibited same overall kinetics and comparable rate.

The morphology and structure of nanoporous metals can be controlled using organic templates. For example, gold and gold–silver alloys have been deposited electrochemically in ion track-etched polymer and smooth gold and gold–silver alloy nanowires were generated [66]. Porous gold nanowires were subsequently obtained by dealloying. The nanoporous gold wires showed the porosity-dependent plasmonic behavior. A strong redshift of the resonant wavelength and significant line broadening were found. The reason for this is due to a lowered average electron density and a higher electron scattering in the porous gold. The sensing performance of the porous gold wires was tested by the surface-enhanced infrared absorption.

Another example of using a template to tune the structure of dealloyed metals is introduced in [67]. A weaved Teflon fiber mat was used as the template for thin-film ruthenium (Ru) and copper (Cu) binary alloys. The Ru–Cu alloys were coated on the Teflon template by co-sputtering of the precious metal: Ru and the nonprecious metal: Cu. The alloys were then selectively dealloyed by using sulfuric acid as the etchant. The resulted porous Ru as the hydrogen generation catalyst was reported.

The complex structure of nanoporous gold wire arrays can be prepared by integrated micro-nanofabrication processes [68]. First, the nodular growth of gold–copper alloys was achieved by magnetron sputtering the alloys on a silicon wafer with a photoresist nanoparticle residue as shown in Figure 4a. The gold–copper metallic nanowires containing hillocks emerging out of the surface can be created as shown in Figure 4b. Then, the copper can be selectively removed by electrochemical dealloying and the resulted morphology is shown in Figure 4c.

Such an approach has been demonstrated applicable to multiple metals and alloys including gold, copper, silver, gold–copper, and gold–silver. It was found that the hillocks can be transformed into the ring-like nanoporous structure by the electrochemical dealloying of the gold–copper alloy nanowire arrays. The resulted porous gold nanowires exhibit a very high roughness and large specific surface area, which makes them a promising candidate for developing advanced sensors.

In view of the metallic hillock formation, it is proposed that there is a region around the photoresist residue where the shadow effect is significant during the sputtering of metal coatings as shown in Figure 5a. The metal deposits may not be able to cover this region due to the deposition

rate difference between the top of the nanodome and the shadow region as illustrated in Figure 5b. The top of the nanodome experienced higher deposition rate than the other region. Therefore, a metallic hillock formed as schematically shown in Figure 5c.

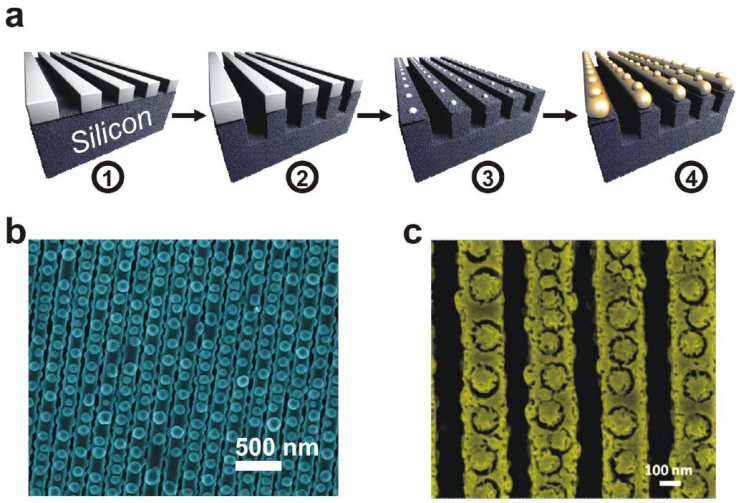

Figure 4. Scheme of metallic nanowire fabrication and the SEM images of nanowires: (a) schematic showing the formation of metallic nanowires on a silicon wafer, (b) SEM image of the prepared metallic nanowires before dealloying, (c) SEM image of the prepared metallic nanowires after electrochemical dealloying [68]. Reprinted (adapted) with permission from Ref. [68].

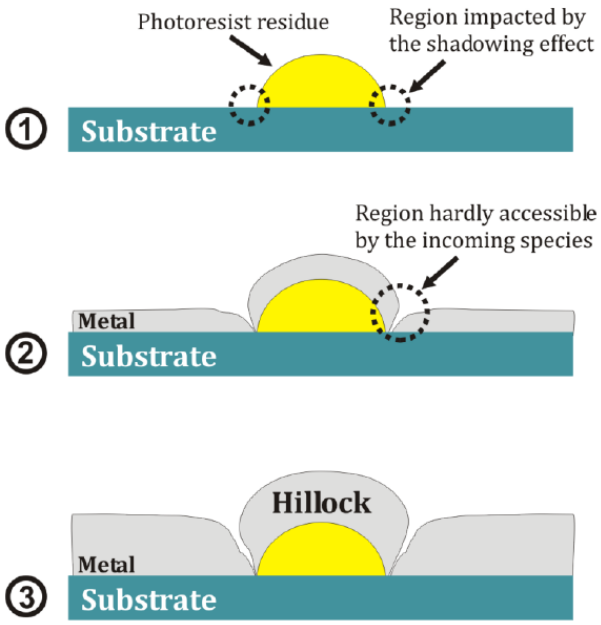

Figure 5. Schematic showing the metallic hillock formation on a photoresist nanoparticle residue: (1) the stage of a photoresist residue formation on the plasma etched silicon wafer, (2) the stage of metal deposition on the plasma etched silicon wafer with the photoresist residue, (3) the stage of metallic hillock formation on the silicon wafer [68]. Reprinted (adapted) with permission from Ref. [68].

Some interesting morphological details are also demonstrated in [68]. When the $Au_{18}Cu_{82}$ alloy was dealloyed by the electrochemical method, the initial gold metal hillock-containing nanowires as shown in Figure 6a were transformed into the ring-containing nanoporous structure as shown in Figure 6b. If the potential for electrochemical dealloying is higher, the fine porous structure as shown in Figure 6c was observed. The hillock feature was gone. When the other alloy with the higher gold composition, $Au_{23}Cu_{77}$, was used in dealloying, the ring-like morphological feature was preserved even if the electrochemical dealloying potential increased from 0.3 to 0.4 V. This indicates that the higher gold content allowed the initial structure to be kept. It was also found that a further increasing of the dealloying potential to 0.5 V resulted in the complete delamination of the gold metal nanowires from the silicon wafer.

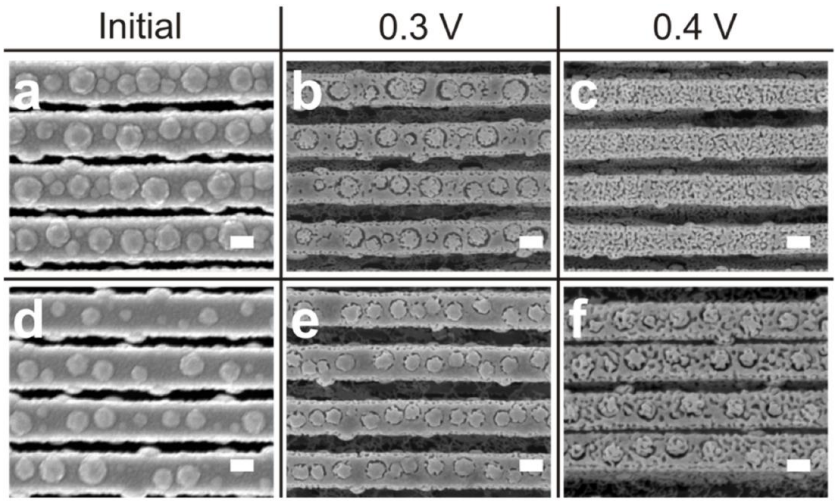

Figure 6. SEM images showing the structure evolution of the metallic nanowires before and after electrochemical dealloying at different scanning potentials: (a–c): $Au_{18}Cu_{82}$ before and after dealloying for 5 min at the potentials of 0.3 and 0.4 V, respectively, (d–f): $Au_{23}Cu_{77}$ before and after dealloying for 5 min at the potentials of 0.3 and 0.4 V, respectively (The scale bar is 100 nm) [68]. Reprinted (adapted) with permission from Ref. [68].

Qiu et al. [69] made a nanoporous metal oxides@metal composite with a high volumetric capacitance. A free-standing nanoporous Ni–Cu–Mn mixed metal oxides on metal with a high surface area was fabricated by chemical dealloying and electrochemical oxidation. The precursor alloy is a $Ni_8Cu_{12}Mn_{80}$ single-phase alloy. After the chemical dealloying in a 1.0 M $(NH_4)_2SO_4$ aqueous solution, the electrochemical oxidation in a 1.0 M KOH solution was carried out. The potential range used for the electrochemical oxidation was from −1.0 to 0.6 V (vs SCE). Experimental results showed that Cu and Mn-based metal oxides formed first by the electrochemical oxidation. Then the Ni-based oxide started growing with the increase in the number of the electrochemical scanning cycles. The Ni-based oxide film, along with the Cu/Mn oxides, formed a relatively stable mixed metal oxide thin film on the metal ligament network.

Microstructure analysis of dealloying multi-phase intermetallic particles was performed [70]. The AA2024 alloy used in the study has a chemical composition of Cu 4.65 wt%; Fe 0.21 wt%; Mg 1.54 wt%; Mn 0.52 wt%; Si 0.088 wt%; Zn 0.11 wt%; Al rem. The microstructure consists of both

theta-phase (Al_2Cu) and S-phase (Al_2CuMg). It was dealloyed by immersion in a 3.5 wt% NaCl solution at the ambient temperature. It was found that the dealloying with selective removal of aluminum occurred preferentially at the S-phase. The de-alloying of the theta-phase initiated in the regions surrounding the S-phase. The selective dissolution of Al from the theta-phase resulted in porous copper-rich theta-phase remnant, consisting of randomly oriented copper metallic particles and copper oxides with sizes of 10–50 nm. Banding structure developed during the de-alloying of the theta-phase particles that contain stacking faults. The de-alloying of the theta-phase could preferentially occur from beneath the alloy surface, associated with the local low pH environment generated by trenching of the alloy matrix in the periphery theta-phase particles.

4. Properties of dealloyed nanoporous metals

4.1. Mechanical property

Mechanical testing on nanoporous metals at the macroscopic scale may only reveal the properties of nanoscale solids in general. However, some important questions in this area should be answered. They are as follows. Can the macroscopic strength and elastic modulus of nanoporous metals be correlated with the properties of nanoscale ligaments [4]? Is a nanoscale network formed in the dealloying similar to that in a traditional metallic foam? Does the network connectivity affect the mechanical response? How do the ligament size and surface properties affect the elastic and plastic response of nanoscale solids? Why is there a tension–compression asymmetry in strength for porous metals? To explore the answers to such questions, observations on the mechanical responses of nanoporous metals with a focus on gold were presented [4]. Due to the porous feature, a dealloyed bulk material is typically weaker than its precursor alloy in view of the mechanical property. In most cases, it is very hard to extract the mechanical property data due to the small scale in size of nanoporous materials. Simulated nanoindentation tests for a model polycrystalline nanoporous gold structure with 11 nm mean filament diameter and 35 nm average grain size, comparable to foams produced by dealloying were performed [71]. The results of hardness were obtained. Plasticity mechanisms were proposed. The extension of the plastic zone was analyzed. The applicability of several scaling laws was discussed as well. The plasticity generally occurs at the nodes. The origin of the plasticity is from the nucleation of dislocations at the atomic steps on the ligament surfaces. In a dislocation accumulation scenario, perfect dislocations, Shockley partials, Hirth partials, Lomer-Cottrel locks and twins were identified. Grain boundary sliding appears to play a minor role in deformation at the indentation rates used. Several scaling laws are tested and their results and applicability are discussed based on the structural parameters of the foam and the deformation mechanisms.

The $Cu_{50}Zr_{45}Al_5$ bulk metallic glass (BMG) has high fracture strength. In order to improve the plasticity and control the mechanical properties of the bulk metallic glass, a surface dealloying was carried out on a 2 mm rod to obtain a solid BMG core and a porous surface layer [72]. The dealloying process was done in a 0.05 M HF aqueous solution at the room temperature of 298 K for one day to five days. In the surface dealloyed layer, the initial solid structure with the composition of $Cu_{50}Zr_{45}Al_5$, was converted to porous copper as can be seen from the color change in Figure 7a. Some Cu_2O was also found at the surface of the porous copper as revealed in Figure 7b. Scanning electron microscopic analysis of the porous surface was performed to examine the porous structure

evolution. With the shortest surface dealloying period of just one day, the surface are full of uniform nanopores as illustrated in Figure 8a. Figure 8b, the SEM image showing the structure after dealloying for three days, revealed an increase in the ligament size. Figure 8c is an SEM image showing the surface structure after dealloying for five days. The size of the ligaments increased further. The energy dispersive X-ray diffraction spectrum of the surface layer in Figure 8d clarified that dealloying left copper as the major element at the surface.

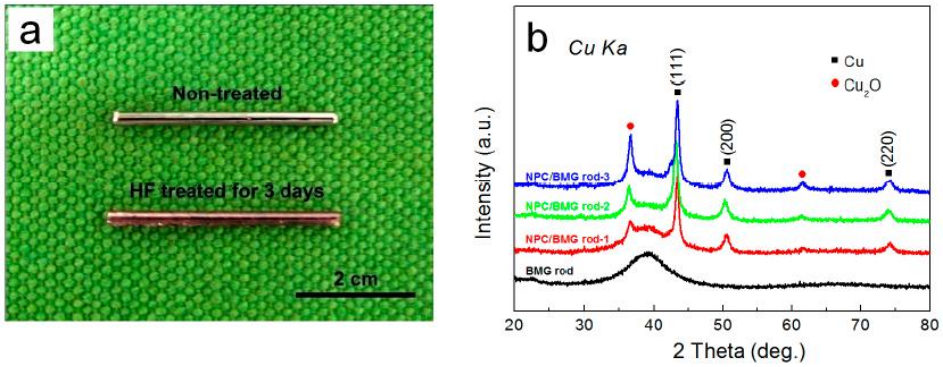

Figure 7. Optical micrograph and X-ray diffraction results of the surface layer: (a) a picture showing the color change due to the selective leaching of Zr and Al from the BMG in HF, (b) X-ray diffraction results of the surface layer confirming the formation of copper-rich phases due to the surface dealloying [72]. Reprinted (adapted) with permission from Ref. [72].

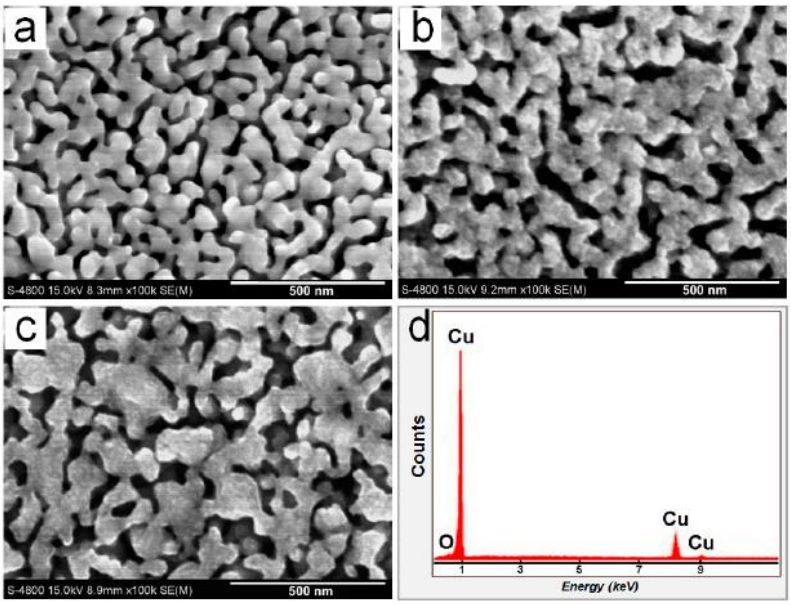

Figure 8. Scanning electron microscopic analysis of the porous surface: (a) SEM image showing the structure after dealloying for a day, (b) SEM image showing the structure after dealloying for three days, (c) SEM image showing the structure after dealloying for five days, (d) energy dispersive X-ray diffraction spectrum of the surface layer [72]. Reprinted (adapted) with permission from Ref. [72].

It is meaningful to reveal the fracture surfaces of the BMG and composite material with a BMG core and a nanoporous surface layer for understanding the failure mechanisms. Figure 9a schematically shows the BMG under a uniform far field compressive loading. Typically, the glassy metal tends to fail easily and the failure of the BMG under such a loading generated a fracture surface as shown in Figure 9b. The vein-like pattern represents a low energy absorption process associated with the fracture of the glass. However, when the composite material with a BMG core and a nanoporous surface layer was subjected to the compressive loading, the glassy core experienced a circumferential compressive load from the confinement of the surface layer as illustrated in Figure 9c. Due to the crystalline structure of the porous copper layer, it has higher plastic deformation capability than the inner glassy core. Figure 9d, the fracture surface consisting of this outer layer and the transition layer, demonstrated much higher roughness than the inner glassy core, which indicates a lot of plastic deformation before failure. Evidently, there is a mechanical shielding effect of the surface layer and the transition layer on the inner core.

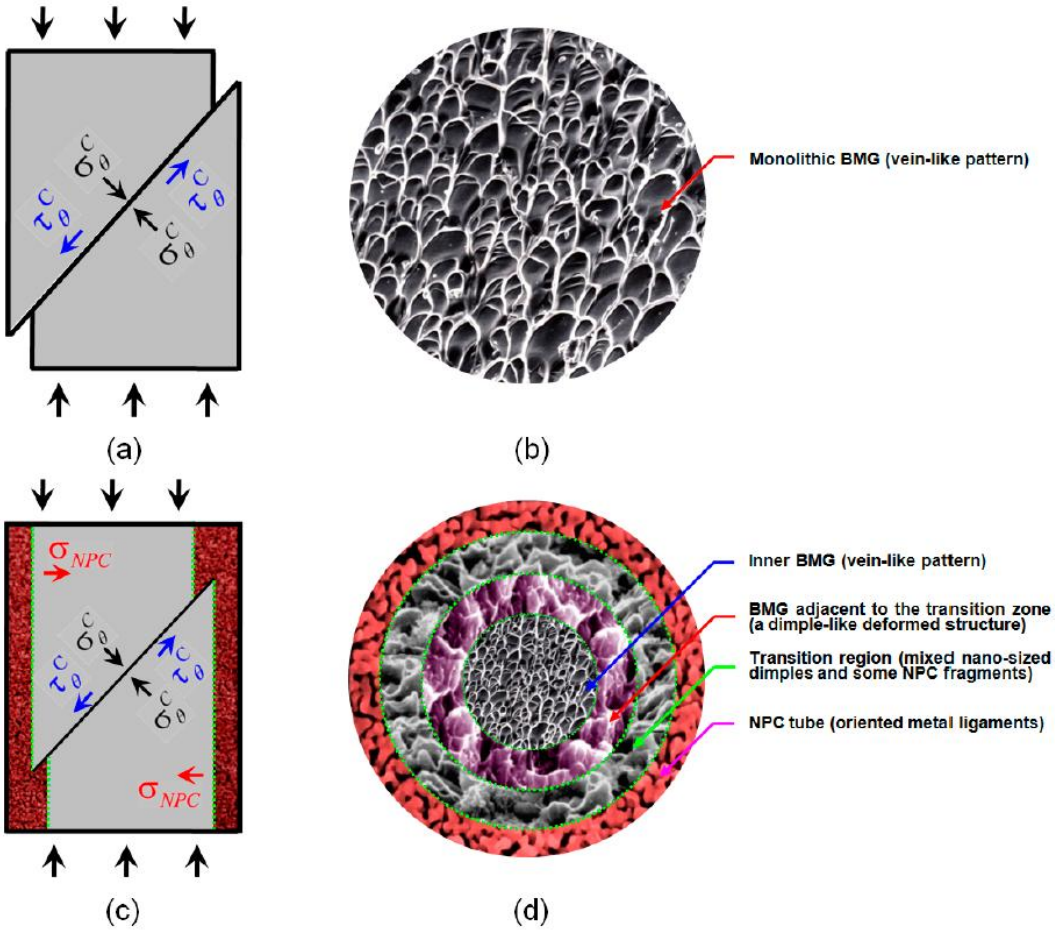

Figure 9. Schematic illustrations showing the stress states and scanning electron microscopic images showing the fracture surfaces of the BMG and the composite failed under compression [72]. Reprinted (adapted) with permission from Ref. [72].

The core of the composite material became the loading bearer. While the surface layer took the crack arresting role. In addition, the outer layer should have a much higher energy absorption

capability than the inner glassy core. This allows the suppression on the shear stress induced crack initiation and propagation in the glassy core. Therefore, the mechanical properties are expected to be improved through this surface dealloying treatment. The mechanical properties of the hierarchical nanoporous copper/bulk metallic glass (NPC/BMG) rods were tested. The composite rods demonstrate significantly enhanced ductility under compressive loadings [73]. The compression strain of 2.9% was achieved for the nanoporous structured NPC/BMG composite rods. While the BMG rods without dealloying only show a ductility of 2.0% under the same loading conditions. The one-pot chemical dealloying of the $Cu_{50}Zr_{45}Al_5$ BMG rods in a 0.05 M HF solution for a day generated a NPC layer with a thickness of 85 μm. The increase in the compression strain confirm the role of the buffer deformation zone resulting from the existence of the outer nanoporous copper layer.

Generally, the surface stress induced axial strain in a fiber-like solid is larger than its radical strain, and is also greater than the radical strain in similar-sized spherical solids. Thus, it is believed that the surface induced macroscopic dimension change (i.e., actuation strain) in nanoporous gold (NPG) increases with decreasing relative density, or alternatively, with an increasing ratio between volumes of fiber-like ligaments and sphere-like nodes. Liu et al. [74] found that there exists an anomalous low strain induced by surface charge in nanoporous gold with low relative density based on their studies on electrochemical actuations of NPG with similar structure sizes, same (oxide-covered) surface state but different relative densities. The responses of the nanoporous gold to surface charging/discharging were tested *in-situ*. It was observed that the actuation strain amplitude did not increase, but decreased dramatically with the decreasing relative density of the NPG. The actuation strain decreased abruptly when the relative density of NPG was decreased to less than 0.25. The Au content in the Au–Ag precursor was lower than 20 at% for the precursor alloy. This anomalous behavior cannot be explained by the potential- or size-dependent elasticity. Rather, the structure difference came from different dealloying rates. Additional strain was induced by the external load during dilatometry experiments. In such a NPG with a low relative density, coordinate movements of nanoscale ligaments may occur in the pore space and disconnected regions, which could offset the total strain in the ligaments. Therefore, an anomalous low actuation strain was found macroscopically. Another anomalous mechanical behavior, i.e., anomalous compliance, was studied by both molecular dynamics and finite element simulations [75]. The elasticity of a nanoporous gold was computed from molecular dynamics (MD) and finite element method (FEM) simulations. The linear elastic FEM simulation gives a substantially stiffer response than the MD simulation. Both models yield much higher compliance values than the predictions of the Gibson-Ashby scaling relation for metal foams. Microstructural features and the porosity are considered as the factors influencing the compliance. Also, the nonlinear elastic behavior contributes significantly to the anomalous compliance of nanoporous gold at the small structure size.

The size effect of ligaments on the charge induced surface stress in nanoporous Pd was investigated by Cao et al. [76]. The nanoporous Pd with different ligament widths (w) were prepared by electrochemical dealloying a $Pd_{20}Co_{80}$ single phased solid solution alloy in sulfuric acid followed by thermal coarsening. The nanoporous Pd samples were generated in a 0.1 M H_2SO_4 for 72 to 120 h at a corrosion current less than 0.025 mA by complete removal of the Co element. The potential scanning ranged from +0.2 V to +0.45 V (vs SCE) during the electrochemical dealloying. The electrocapillary coupling parameter, ζ, which is usually used to quantify the charge induced surface stress response, of the as-prepared samples was measured by an *in-situ* dilatometry method. According to Weismüller et al. [77–80], ζ can be expressed as:

$$\zeta = -\frac{9Km}{2\rho l_0}\frac{\Delta l}{\Delta Q} \tag{10}$$

where m and ρ denote the sample mass and the mass density of the porous material, respectively. l_o is the initial sample length. The macroscopic strain can be calculated by $\Delta l/l_o$. ΔQ is the transferred charge. It is found that when w is smaller than a critical value of 49 nm, the ligament size effect is significant. The absolute value of ζ increased from 0.76 V to 1.03 V with the decreasing of w. But if w is larger than the critical value, the ligament size effect on ζ is negligible.

The strength of nanostructures could be higher than the associated precursor alloys. Usually, replacing parts of a solid with voids weakens a material. However, the size effect is complicated and could result in the unusual increase in the strength of material. Ye and Jin [81] reported that it is possible to make an Au–Pt–Ag alloy nearly seven times stronger than the precursor by dealloying. Its strength increased from 50 to 345 MPa, when approximate to 40% of solids (Ag) was dissolved and replaced by pores during the electrochemical dealloying at 1.04 V (vs SCE) in a 1.0 M $HClO_4$ solution. The corrosion-induced strengthening originates from the formation of nanoporous structure, and the high strength of nanoscale ligaments is due to the size effect. Nevertheless, the connectivity of the nanoporous structure decreases during the pore and ligament coarsening, which caused the decreases in both strength and stiffness. That is why for most nanoporous gold materials, only low strength and stiffness were obtained. Although post annealing nanoporous materials leads to the ligament structure coarsening and reduces the strength of the materials, there are some exceptions. A gold nanostructure mat is such an example [82]. The gold mat was made of gold nanoparticles through a simple, inexpensive self-assembly process via a bottom-up approach. The mechanical strength of the nano-cluster network can be increased by a post-assembly annealing process.

4.2. Surface activities

Due to the large amount of surface atoms, dealloyed porous metals show high surface activities in catalysis [83,84], chemical adsorption [85], organics oxidation [86], lithium ion storage [87], and bone regeneration [88]. The surface activity of bulk metallic glasses can be enhanced significantly by dealloying. In [83], the catalytic activities of two dealloyed, Pd-rich materials were shown. The nanoporous metals (NPMs) were prepared from $Pd_{10}Ni_{70}P_{20}$ and $Pd_{10}Ni_{50}Co_{20}P_{16}B_4$ metallic glasses. These two alloys were potentiostatically dealloyed in an acid solution. The pore size of the as obtained NPMs is about 100 nm. The NPM dealloyed from $Pd_{10}Ni_{70}P_{20}$ kept the same elements, but the composition changed into $Pd_{89}Ni_8P_3$. The other NPM dealloyed from $Pd_{10}Ni_{50}Co_{20}P_{16}B_4$ has a composition of $Pd_{85}Ni_{11}Co_3P_1$. Due to the increase surface activities, both of the Pd-rich NPMs exhibit lower formic acid electro-oxidation potential when compared with the commercial Pd/C catalyst. The low formic acid electro-oxidation potential indicates enhanced catalytic activity toward formic acid oxidation. The Ni and Co residuals from the dealloying contribute to the surface activities of the NPMs because Ni and Co locate in the lower unoccupied molecular orbits of the Pd clusters, which increases the catalytic activity of the nanoporous metals. Pd-based alloys are also important catalysts for the application in direct alcohol fuel cells. There are two major reasons of considering Pd. It has the excellent electro-catalytic performance and relatively low cost. In Wang, Zhang, and Liu's work [84], a nanoporous Pd-rich structure was made from the electrochemical dealloying of the $Pd_{32}Ni_{48}P_{20}$ metallic glass in a 0.5 M sulfuric acid solution. The dealloyed material consisted of amorphous nanoparticles and interconnected conduits. This material exhibited an

enhanced catalytic activity towards to the methanol electro-oxidation in a 1.0 M methanol solution containing 1.0 M potassium hydroxide (KOH). The increase of the surface activities comes from the synergy of amorphism and high porosity of the dealloyed nanoporous alloy.

Controlling the interface structure of porous materials provides a new approach to new functional materials. The functions include electrochemical potential switching of strength, stiffness, fracture resistance, fluid sorption, actuation, and quasi-piezoelectric strain sensing as discussed in [85]. Dealloying can tune the characteristic structure size down to a few nanometers. At such a small scale, some desired interface-controlled behavior of nanoporous materials can be obtained. Indeed, both the pore and the ligament sizes can be readily tuned to the range from a few nanometers to several microns. At the nanoscale, those porous structures are typically in a network of ligaments with well-defined characteristic sizes. The porous structures can also be prepared into macroscale dimensions prior to the dealloying process. Such hierarchical structures can be made into functional components. Their active surface area is very large and the bicontinuous feature provides transport channels and paths, which enhances the surface activities. It is also possible to change the surface states by controlling the electric or chemical potential. Such dealloyed porous materials create new opportunities for exploring the effects of surfaces on material behaviors and for using the surface effects in novel functional materials design strategies. Experiments on the surface effects involving small-scale plasticity and elasticity have been demonstrated as well [85].

The high surface activity of a nanoporous copper has been found useful in the oxidation of organic compounds, for example, electrocatalytic oxidation of $(CH_2OH)_2$ [86]. The bi-continuous and uniform nanoporous copper was prepared via chemical dealloying the quaternary amorphous alloy: $Zr_{65}Cu_{17.5}Fe_{10}Al_{17.5}$ in hydrofluoric acid (HF) solutions with different concentrations. A three-dimensional bi-continuous nanoporous copper (NPC) structure was obtained. The pore size of the dealloyed material ranges from 45 nm to 58 nm. It was noticed that the pore size of the nanoporous copper structure increased with the increase of the dealloying time. The cyclic voltammetry (CV) results reveal that the nanoporous copper has the high surface activity to oxidize the $(CH_2OH)_2$ solution. The precursor amorphous ribbon is not surface active for electrocatalysis because there is no oxidation peak on the CV curve.

Dealloying a melt spun Co–Al–Fe amorphous alloy generated bimetallic oxide $CoFe_2O_4$ nanoplates with a porous structure. The dealloying was performed in NaOH solution by selective removal of the Al element. The electrochemical properties of the dealloyed porous material were investigated as an anode material for Li-ion batteries. The material presented stable cycling properties with a reversible capacity of 1280.8 mAh/g after 100 discharge/charge cycles at a current density of 500 mA/g, and a reversible capacity of 810 mAh/g after 1000 discharge/charge cycles at a current density of 2.0 A/g, among one of the best performance of the reported $CoFe_2O_4$ anodes. The interconnected sheet-like micro/nanostructure with plenty of space improved Li storage properties. In addition, the dimension stability reduced the tendency to cracking and kept the low electrical resistance during the charge–discharge cycles.

To increase the surface activity for bone generation, porous Ti_xHf_{100-x} alloys were processed first through the liquid metal dealloying Ti–Hf–Cu precursors in molten magnesium. Then, interpenetrating-phase metal–polymer composites mimicking the mechanical behavior of cortical bone were made. The composites show intermediate strength and low stiffness close to the mechanical properties of the bone. The structures of the composites consist of dealloying-based open porous Ti_xHf_{100-x} alloys (scaffolds) impregnated by a polymer named bisphenol F epoxy resin (BPF).

The porous metal scaffolds significantly contribute to strength (215–266 MPa) and stiffness (15.6–20.8 GPa) of the composites while the polymer phase provides the high strain rate sensitivity (0.037–0.044). Tuning scaffolds' connectivity by preloading and/or their chemical composition allows the fine adjustment on composites' mechanical properties. The results suggest that the composites should have potential for implant material applications [88].

4.3. Catalytic property

A dealloyed nanoporous gold (NPG) has been used as the substrate for the deposition of palladium for catalytic applications [89]. The prepared nanoporous catalyst was found very efficient in catalyzing the oxygen reduction and oxygen evolution reactions. The oxygen reduction and oxygen evolution reactions are considered as the important processes for fuel cells, metal-air batteries, and water splitting systems. Through the surface modification on the dealloyed nanoporous gold, a Pd surface layer was uniformly deposited onto the nanoporous gold ligament surface via the epitaxial growth. As compared with the traditional Pt/C catalyst, the new NPG–Pd nanocatalyst exhibited the enhanced electrocatalytic activities in the oxygen reduction and oxygen evolution reactions. The remarkable catalytic performance of the new catalyst is believed due to the unique three-dimensional nanostructure of the NPG, resulting in the efficient utilization of the Pd layer on the gold ligaments. The density functional theory calculations revealed a change in the electronic structure in the Pd/Au nanostructure. Such an electronic structure change enhanced the electrocatalytic behavior of the NPG–Pd porous material.

In order to make a nanoporous Pd/NiO composite catalyst, a melt-spun $Al_{85}Pd_{15}$ precursor alloy with trace amount of Ni was dealloyed in a 20 wt% NaOH solution at the ambient temperature for selective removal of the aluminum element [90]. The resulted nanoporous catalyst was tested for methanol oxidation in alkaline media. The morphology analysis revealed a uniform bicontinuous and interpenetrating three-dimensional nanoporous structure. Pore channels with a length of less than 10 nm ran all the way throughout the thickness of the sample and the pore wall was observed in the ligament-like shape. Energy dispersive X-ray diffraction spectrometry measurement indicated that the ligament consisted of Pd, Ni, O, and residual Al. The possible oxidation states of Ni and Pd were determined by the XPS spectrum. All the Ni atoms were oxidized and the oxidation product was NiO. The electrocatalytic activities of the nanoporous Pd/NiO composite was evaluated. Better electrocatalytic performance for the composite was found as compared with pure nanoporous Pd. One of the best results showed that the electrocatalytic efficiency of the composite catalyst was about 4 times as high as that of the pure nanoporous Pd. It is concluded that the improvement of the electrocatalytic property is due to the increased electrochemically active specific surface areas. The synergistic effect between Pd and NiO also contributes to the enhanced catalytic activities.

The electrocatalytic activities of nanoporous Au–Cu with ultrafine ligaments towards glucose oxidation and hydrogen peroxide reduction depend on the ratios of the Au:Cu. In order to tune the composition of the nanoporous Au–Cu, a two-stage dealloying was reported [91]. Basically, the nanoporous Au–Cu was prepared from the chemical dealloying of a single-phased $Au_5Cu_{25}Mn_{70}$ alloy in a 1.0 M $(NH_4)_2SO_4$ solution. The dealloying process can be divided into two stages. The first stage refers to the removal of Mn from the precursor alloy. In the second stage, a slow etching of Cu to tune the ratio of Cu to Au on the Au–Cu nano-ligament surface was carried out. It was found that the optimized composition is Au:Cu = 66:34. Its high electrocatalytic activity was confirmed by

oxidation of glucose and reduction of hydrogen peroxide. The results indicate that the prepared the nanoporous $Au_{66}Cu_{34}$ alloy can be used as both an anode and a cathode catalyst for glucose fuel cells.

Dealloyed nanoporous metallic materials have been studied for hydrogen combustion catalysis [92]. First, Pt–Cu thin films were deposited on a SiC substrate by magnetron sputtering. Then, chemical dealloying on the Pt–Cu to remove Cu from the films was performed. Tests on the dealloyed films for use as catalysts during the combustion of hydrogen under oxidizing conditions were carried out. Comparative studies were made by testing the catalysts as prepared and after chemical dealloying. The as-prepared Pt–Cu thin films showed significant activity only at temperatures higher than 100 ℃. But the dealloying allowed the increase in the activity at the ambient temperature.

Porous alloy nanowires with rugged ligaments were prepared for the enhanced electrocatalysis [93]. The nanoporous catalysts were made from Pt–Au–Cu alloys. The final products of porous nanowires with the diameters ranging from 200 to 500 nm were obtained by removing Cu from the alloys in an 8.0 M nitric solution. Due to the large surface areas and a high density of defect sites within the porous nanowires, the high electrochemical catalytic property for the oxygen reduction reaction (ORR) in fuel cells was found. The scalable one-step dealloying approach was also used to prepare nanoporous alloy nanowires with controllable compositions. The effects of grain size, structure, and composition of the Pt–Au–Cu precursor alloys on the formation of the porous nanowires were investigated. It has been found that the formation of separated nanowires is due to the large-scale shrinkage of the column-structured grains during dealloying of Cu, which also generates ultrafine nanopores and rugged alloy ligaments with a high density of defect sites in the nanowires. When used as a cathodic catalyst for the oxygen reduction reaction, the PtCuAu nanoporous nanowires exhibit a composition-dependent catalytic performance. The dealloyed nanowires show more than 14 times higher efficiency than that of commercial Pt/C as cathodic catalysts for fuel cells.

In addition to nanowire catalysts, nanorods were prepared for catalysis. The monolithic Au/CeO_2 nanorod frameworks (NFs) with a porous structure were obtained by dealloying melt-spun $Al_{89.7}Ce_{10}Au_{0.3}$ ribbons. The nanorods were used as catalysts for low-temperature CO oxidation. After dealloying, the ribbons were heat treated at 400 ℃ in O_2 to form porous 3D Au/CeO_2 NFs with large surface areas. Small Au clusters and nanoparticles (NPs) were dispersed on the nanorod surface, creating many nanoscale contact interfaces. Oxygen vacancies were also found with a high concentration in the heat treated sample. The calcined Au/CeO_2 nanorod catalyst exhibited much higher catalytic activity for CO oxidation compared with the dealloyed sample and bare CeO_2 nanorods. It is concluded that the Au/CeO_2 NF catalyst exhibits high catalytic performance owing to the enhanced interaction between the Au clusters/NPs and CeO_2 nanorod during calcination [94].

Computational studies on the dealloyed noble metals for catalysis were conducted. For example, Zhang et al. [95] did the first principles calculations for the dealloyed nanoporous gold and showed that gold atoms with low generalized coordination numbers possessed high activity for electro-reduction of CO_2 to CO. Atom-resolved three-dimensional reconstruction was also performed and the results revealed that dealloyed nanoporous gold had the favorable structure and characteristics for maintaining a high faradaic efficiency of 94% during the reduction of CO_2 to CO.

Hierarchical nanoporous platinum–copper (hnp-PtCu) alloy nanoflowers with bimodal pore/ligament size have high catalytic activities toward the hydrolysis of ammonia borane (AB) [96]. The nanoflowers were made by selectively dissolving Al atoms and part of Cu atoms from a Pt–Cu–

Al ternary alloy. There are several structural features in the dealloyed samples including cross-linked porous nanoflowers, interconnected network skeletons, and interpenetrating hollow channels. As compared with their monometallic components, the hnp-PtCu alloy nanoflowers with different compositions exhibit dramatically enhanced catalytic activities. The hnp-$Pt_{35}Cu_{65}$ alloy shows superior catalytic performance than the other hnp-PtCu catalysts. Moreover, the hnp-$Pt_{35}Cu_{65}$ displays excellent structure stability even after the five runs for the AB hydrolysis.

A nanoporous Ir/IrO_2 anodic water electrolyzer catalyst was made by electrochemical dealloying of osmium from an $Ir_{25}Os_{75}$ alloy at 1 mA/cm^2 in 0.1 M $HClO_4$ at 25 ℃ [97]. The Ir/IrO_2 catalyst shows a proper balance between activity, stability and conductivity for catalyzing the oxygen evolution reaction in acid-based electrolytes. The structure of the catalyst consists of a highly conductive nanoporous architecture of an iridium oxide shell and an iridium metallic core, which is the origin of an exceptional balance between oxygen evolution activity and stability as quantified by the activity-stability factor. Due to its optimized stability and conductivity, the nanoporous Ir/IrO_2 shows near 30 times improvement in activity-stability factor relative to conventional iridium-based oxide materials, and 8 times improvement over dealloyed $Ir_{25}Os_{75}$ nanoparticles, respectively.

Efforts have been put on understanding the origin of the high catalytic activity of dealloyed nanoporous metals in the dry reforming of methane gas and carbon dioxide. The dry reforming is meaningful because it sequestrates carbon dioxide while at the same time generates hydrogen gas in an economic way. Fujita et al. have studied the dry reforming of methane using a dealloyed nanoporous Ni–Co catalyst [98]. It is found that the chemical dealloying of Ni and Co and grain refinement generated synergic effects for increasing the catalytic activity. Non-Pt based electrocatalysts, for example, a dealloyed $PdBi_2$ alloy, facilitate hydrogen evolution reactions [99]. Synthesis of $PdBi_2$ was carried out using sodium borohydride as the reducing agent. Upon annealing the as-synthesized $PdBi_2$, a phase transformation from the lower symmetry monoclinic phase to the higher symmetry tetragonal phase was observed. The material changed into a core–shell structure. Potential electrochemical cycling of both monoclinic and tetragonal $PdBi_2$ leads to the formation of a Pd-rich $PdBi_{2-x}$ alloy with enhanced catalytic activity. Structural transitions and metal deficiency generation are the effective ways of manipulating the *d*-band center of Pd surface, which enhances the catalytic activity of Pd–Bi towards the hydrogen generation. Charge-transfer from *in-situ* generated oxide specie (Bi–O) to the Pd center also leads to the increase of catalytic activity towards the hydrogen production.

Residual silver, left in the sample after dealloying of a gold–silver alloy, has been shown a strong influence on the activity of the catalyst [100]. The residue silver was found to form clusters that are distributed irregularly, both at the surface and inside the gold ligaments building up the porous structure. CO oxidation is promoted by more residual silver, but methanol oxidation to methyl formate is hindered. The exact role of the residual silver remains to be determined. Dealloyed gold may serve as the support for catalysis. In [101], nanoscale tungsten disulfide/poly(3,4-ethylenedioxythiophene) (PEDOT) was electroplated onto the surface of a dealloyed nanoporous gold (NPG) to generate a uniform nanocomposite. This composite offers an excellent electrocatalysis performance for hydrogen evolution reaction (HER) in acidic media. PEDOT itself is inert for the HER, but was found to improve the conductivity and operating stability of the WS_2 catalyst significantly.

4.4. Mass, electron and phonon transport properties

Due to the porous feature, dealloyed materials are expected to have some unique transport properties including mass transfer, electron transport and phonon transport properties [1]. Therefore, some characteristics such as fast diffusion through the pores, high electrical conductivity from the ligament networks, and low thermal conductivity due to the phonon scattering from the high surface and interface areas could be demonstrated by dealloyed materials. Improving the electrical conductivity of electrode materials has a positive influence on the charge–discharge reversibility of rechargeable batteries. Nanoporous silicon/copper (NP-Si/Cu) composite is one of the candidates for lithium ion battery anode material [102]. The Nanoporous (NP) Si/Cu composite was through alloy refining followed by a chemical dealloying process. The composite showed a three-dimensional porous network nanostructure. The Cu content can be changed by varying the feeding ratio of alloy precursors. By integrating the conductive Cu into a nanoporous Si backbone, the NP-$Si_{85}Cu_{15}$ composite exhibits enhanced electrical conductivity. Due to the high porosity in the composite, reduced volumetric expansion and fracture during repeated charging-discharging processes in lithium-ion batteries (LIBs) were achieved. Consequently, the nanoporous composite possesses much higher cycling reversibility than the pure NP-Si.

As an alternative method for generating nanoporous metals, the electrochemical dealloying approach has been used to make 3D nanoporous copper as the current collectors for dendrite-free Li metal anodes [103]. The 3D porous copper (Cu) current collectors have several advantages. First, the high conductivity of copper allows the internal power loss to be low. Second, as a host for Li deposition, the porous copper can effectively suppress the lithium dendrite growth problem during the charge–discharge cycling. The electrochemical dealloying a Cu–Zn alloy precisely engraved a 3D Cu structure with uniform, smooth, and compact porous network. Such a continuous structure allows the 3D Cu to have excellent mechanical properties and high electrical conductivity. The uniform and smooth pores with a large internal surface area ensures well dispersed current density for homogeneous Li metal deposition and accommodation. A smooth and stable solid electrolyte interphase is formed and meanwhile Li dendrites and dead Li are effectively suppressed. The Li metal anode conceived 3D Cu current collector can stably cycle for 400 h under a Li plating/stripping capacity of 1 mAh/cm^2 and a current density of 1 mA/cm^2. The Li@3D Cu||$LiFePO_4$ full cells present excellent cycling and rate performances.

In a recent review performed by Fujita [104], the generation of 3D hierarchical pores in Au–Ag alloys was discussed and schematically shown. As shown in Figure 10, multiple dealloying procedures were carried out to generate the hierarchical porous structure. The multiple dealloying procedures include the dealloying/plating/ligament and pore expansion/re-dealloying multiple steps as described in more details in [105]. In the first dealloying step, two precursor Au–Ag alloys: $Au_{35}Ag_{65}$ and $Au_{10}Ag_{90}$, as shown in the upper left part of Figure 10, were etched to partially remove the Ag element in the two alloys. The obtained two porous alloys are $Au_{95}Ag_5$ and $Au_{35}Ag_{65}$, as illustrated in the upper right hand sketch in Figure 10. The porous $Au_{35}Ag_{65}$ was annealed thermally to expand the pores. The porous $Au_{95}Ag_5$ was deposited with silver by plating [105]. After silver plating, the composition of the alloy reached $Au_{35}Ag_{65}$. Then, the pore expansion was also performed for this silver deposited alloy, as revealed by the sketch in the lower right hand part of Figure 10. A second step of dealloying was conducted to generate the fine pores within the $Au_{35}Ag_{65}$ ligaments. It was shown that the second dealloying step could remove the Ag element completely if necessary to

reach a lower hierarchical level in the form of nanopores inside the larger gold-rich ligaments [106]. The final products from the two ways are the same, i.e., hierarchical porous $Au_{35}Ag_{65}$, as shown by the sketch in the lower left part of Figure 10. The obtained $Au_{35}Ag_{65}$ has a three-dimensional (3D) structure of randomly interpenetrating ligaments/nanopores with sizes ranging from 5 nm to several tens of micrometers. The ligament size and the pore size can be fine-tuned by varying the processing conditions including the dealloying time, temperature, and additional thermal coarsening parameters. As compared to other nanostructured materials, more controllable transport properties can be obtained for this 3D hierarchical porous alloy. First, the good electrical conductivity was achieved. Second, the pores with a large size than 1 micron promoted fast mass exchange due to the smooth mass transport behavior. It must be noted that the mass transport in nanopores are impeded because there is a very high resistance to the laminar flow due to the capillary effect in the pore with the sizes smaller than 1 micron. Low thermal conductivity is another characteristic property of the hierarchical porous material. Since the micropores could be the sites for strong phonon scattering, the heat transfer in such materials could be significantly slower than other nanoporous metals without such a structure hierarchy.

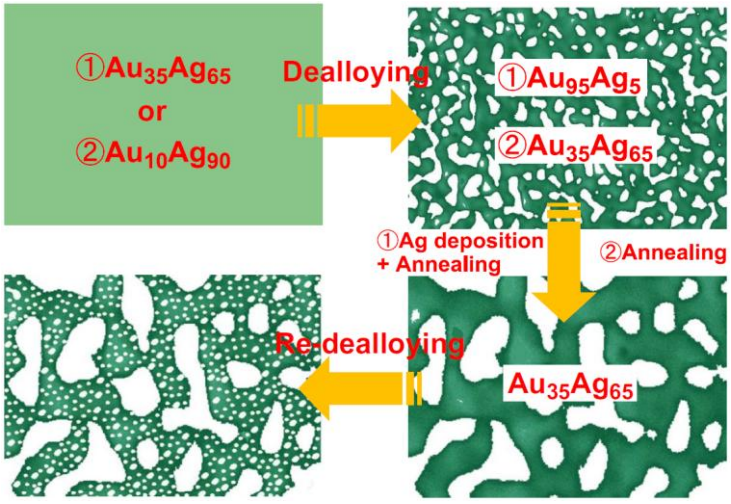

Figure 10. Schematic of multiple step dealloying Au–Ag to form hierarchical porous structures [104]. Reprinted (adapted) with permission from Ref. [104].

4.5. Optical property

Nanoporous metals have unique optical properties such as strong upconversion photoluminescence, enhanced Raman scattering, and surface plasmonics. Upconversion photoluminescence refers to the phenomena that the sequential absorption of two or more photons results in the emission of light at a shorter wavelength than the excitation wavelength. In the work performed by Qin et al. [107], three-dimensional mesoporous gold films were prepared by dealloying gold–silver alloys to increase the upconversion photoluminescence efficiency. The dealloyed Au films were uniform and highly porous, while maintained their chemical stability. Varying the time of the dealloying process led to the change in the pore size distribution, surface roughness, and residual Ag content. The wavelength of the broadband localized surface plasmon resonance (LSPR) can be tuned. The enhancement factor was identified as a function of the dealloying time. With the

optimized upconversion photoluminescence enhancement, a 41-fold increase was achieved with the mesoporous gold made by dealloying for 8 days. The films with an improved upconversion efficiency have potential applications in life science.

The large specific area and strong surface plasmon resonance (SPR) effect allow nanoporous gold suitable for high-sensitivity SPR sensors. Theoretical study on the SPR effect of nanoporous gold films (NPGFs) was conducted [108]. The dispersion relation was obtained for propagating surface plasmons at the NPGF/air interface. The thickness of NPGFs required for optimizing the SPR sensing performance was determined to be 60 nm. For the experimental validation, a large-area, uniform thin NPGF was prepared by a two-step approach involving the sputter coating followed by the chemical dealloying. The obtained nanoporous film has a porosity of 38%, which was determined by fitting the measured resonance wavelengths based on a combination of the Fresnel formula and the Bruggeman dielectric constant approximation theory. The SPR resonance band in the visible-near-infrared region and the sensing properties of the NPGF were measured with the Kretschmann prism-coupling configuration. It must be noted that the prism coupling in the Kretschmann configuration is a well-known method for excitation of surface plasmon polaritons (SPP's) in a metal film bounded from one side by a prism and from the other side by air. The unmodified NPGF is hydrophilic, which allows the accumulation of bisphenol A (BPA) on the surface. The NPGF-SPR sensor can easily detect BPA in water at a low concentration of 5.0 nM.

5. Applications

In this section, the applications of dealloyed porous metals are dealt with. Nano-porous metals offer great potential for applications such as bio-sensors, chemical reactors, platforms for cell growth, and media for separation because of their high surface area and reactivity at the nanoscale. The high surface to volume ratio of nanoporous metals also offers advanced plasmonic properties which may be put to use upon refining the control over pore size distributions in the nanoscale range. Refining the porous structures at the nanoscale and fine tuning their surface properties could further extend their applications. For example, by controlling the temperature of the etchant solution during a 75 min period of chemical dealloying, both ligaments and pores generated across the thin Au–Ag metal leaves can be tuned in view of the dimension [109]. The pore size changed from 30 to 54 nm when the temperature was changed in the range from 5 to 60 ℃. Another significant aspect is that the dealloyed alloys could be tuned in hierarchical structures to simulate those biological tissues as found in wood and bone [110]. It is also realized that the deformability of dealloyed porous materials is critical for some specific applications. The good deformability allows a dealloyed porous material to avoid premature failure when it is experienced with stress concentrations or exposed to the required service loading. So far, most of the nanoporous noble metals such as Au, Pd and Pt can be made deformable. For less precious metals, such as nanoporous Cu–Ni has been made deformable as well [111]. The nanoporous copper–nickel was made as large as in the millimeter size with a uniform bicontinous network structure. The pore size was controlled in the range from 13 to 40 nm through thermal annealing after dealloying. Potential applications are discussed as actuators, sensors, catalysts, microfluidic pumps, bioanalytical systems, and structural materials with tunable mechanical properties. Porous metal material powders with microwave absorption application were studied in [112]. Controlling the pore size by adjusting the reaction condition and varying the composition of a nickel–aluminum nanoparticle precursor was introduced. The porous Ni

nanoparticles (NPs) of 22 nm by chemical dealloying were obtained. A passivation process followed by the dealloying caused the formation of a NiO shell on the porous nickel nanoparticle core. Due to the NiO shell generation as the result of surface oxidation, the pore size can be tuned in the range from 0.6 to 1.2 nm in diameter with a large surface area of 68.9 m^2/g. The selective removal of Al atoms from the precursor during dealloying process reduced the crystalline size of the nanoparticles to 2–5 nm. The low microwave reflection and wide absorption bandwidth are considered mainly from the small pore size and the special core–shell architecture of the porous Ni/NiO NPs. Although it is hard to list all the functions of dealloyed porous metals, for clarity, their applications in several typical fields are presented below with the emphasis on resolving energy, biomedical, and environmental issues.

5.1. Energy storage

How to overcome the lithium storage barriers of current lithium-ion batteries is a big challenge. Conventional low capacity graphite anodes should be replaced by other higher capacity anode materials. Among various candidate materials, silicon is considered as a promising alternative anode material due to its huge energy densities. However, the biggest issue is the lithium-concentration-dependent volumetric change induced performance degradation of capacity during the recharge–discharge cycling. Sohn et al. [113] suggested dealloying Si–metal alloys to fabricate high-performance porous Si anode materials. A wet alkaline chemical etching process was adopted to control the pore development in Si, which allows the establishment of a 3D networking structure. This structure was found enhancing the lithium storage property of the Si-based material significantly. The porous silicon can be used not only in pure form, but also in a graphite-blended composite form.

To increase the sodium storage capacity, nanoporous tin was prepared by dealloying [114]. Controlling the ligament shape in nanoporous tin (NP-Sn) formation during dealloying by free corrosion was able to get nanowires and granular ligaments through adjusting the pH of the corroding solution, and thus the rate of Sn oxidation relative to the etching rate of the sacrificial component. The standard nanowire structure was formed under acidic conditions where oxidation was slow, but a hierarchical granular structure was formed when fusion of the Sn nanocrystals was inhibited by surface oxidation. The materials with two different structures were tested as Na-ion battery anodes. The initial Na storage capacities from 500 to 550 mAh/g were obtained in the nanowire and granular materials, respectively. But the cycle life of the two materials was quite different. The NP-Sn with a granular ligament shape showed enhanced stability with a capacity retention of 55% over 95 cycles at a specific current of 40 mA/g. By contrast, the NP-Sn with the nanowire shape showed very fast degrading in the capacity within the first 10 cycles. It is concluded that there is dramatic impact of the nanoscale morphology on the electrochemical performance of nanoporous materials. Both shape and size controls in dealloyed nanoporous metals are important. Another work on sodium ion batteries (SIBs) also demonstrated the high capacity and low sodiation potential of the dealloyed nanoporous tin [115]. Also addressed in the paper is the inferior cycling performance caused by severe volumetric change and pulverization during the de-sodiation process. To improve the cycling property, a new strategy was proposed to make nanoporous bismuth (Bi)–antimony (Sb) alloys by dealloying of Mg-based ternary alloy precursors. It is found that an SIB anode made from the nanoporous Bi_2Sb_6 alloy has an excellent cycling performance. Due to the

porous structure and proper Bi/Sb atomic ratio, the 10,000 cycling at 1 A/g only caused a capacity decay of 0.0072% per cycle.

The area capacity and cycling performance of nanoporous tin anode for lithium batteries were improved by introducing a bimodal porous current collector with high open porosity and good mechanical stability [116]. The 3D bimodal porous current collector with large interconnected spherical channels of 100–200 μm and nanopores of 100–150 nm was manufactured by the molten-metal infiltration and dealloying. It is found that the Sn coated bimodal porous composite electrodes with good mechanical stability exhibit higher areal capacity and cycling stability than other bimodal porous electrodes and the planar electrodes. In addition to porous tin anode, three-dimensional (3D) hierarchical porous CoNi/CoO/NiO composites were designed and made by selective dealloying aluminum element from an Al–Ni–Co quasicrystalline (QCs) alloy [117]. The CoNi/CoO/NiO electrode was found to have the excellent conductivity coming from the precursor alloy. The strong stability of CoNi was kept. The high theoretical capacities of CoO/NiO was also obtained because of the 3D hierarchical porous structure. As the anode materials for lithium-ion batteries (LIBs), the CoNi/CoO/NiO nanoporous composites showed a high specific capacity of 578 mAh/g at a current density of 200 mA/g after 600 cycles. A similar dealloyed bicontinuous nanoporous NiCoCuY metal/metal-oxide composite was made by the one-step dealloying the $Al_{85-x}Ni_6Y_6Co_3Cu_x$ (x = 1, 3 and 5) metallic glasses in alkaline solutions. The electrochemical performance of the nanoporous composites as binder-free electrodes has been evaluated. It is found that 3 at% Cu addition can achieve the largest capacitance which is attributed to the increase in the electric conductance. The capacitance of nanoporous composites can reach as high as 1.22 F/cm^2 when the $Al_{82}Ni_6Y_6Co_3Cu_3$ sample was dealloyed in a 4.0 M KOH for 50 min. Such a one-step strategy of dealloying metallic glass not only generates a promising functional material for energy storage, but also provides a facile way for decreasing the resistance of electrode material [118].

Nanoporous gold has been studied for the application in the high-energy-density rechargeable lithium ion batteries [119]. A hierarchical and bicontinuous nanoporous gold was constructed by introducing secondary nanopores into the coarsened nanoporous gold ligaments by two-step dealloying. The hierarchical and bicontinuous nanoporous gold cathode provides high porosity, large active surface area and sufficient mass transport paths for high capacity and long cycling lifetime of the batteries. Porous copper has also found applications in energy storage. For example, a 3D porous Cu current collector has been made through chemical dealloying a commercial brass ribbon by selective removing Zn from the Cu–Zn alloy. The interpenetrating pores and the interlinked porous ligaments are integrated naturally in the dealloyed specimen. Such a structure allows the porous material to accommodate Li deposition. The dendrite growth of lithium was suppressed effectively. Consequently, the tendency for volume change during cycling was reduced. It is concluded that the Li metal anode with such a porous Cu collector has excellent performances and commercial potentials in Li-based secondary batteries [120].

5.2. Energy generation

In this subsection, a brief discussion on the application of dealloyed porous metals for clean energy is presented. The first example is for hydrogen generation. The second one is for solar energy harvesting to electricity conversion application. The development of efficient water oxidation catalysts is essential for the economic clean energy generation in the form of hydrogen fuel via

electrolytic water splitting. A Ni–Fe–O-based composite with a unique mesoporous nanowire network structure has been designed and synthesized based on an eutectic reaction and dealloying [121]. The composite showed a very low overpotential, small Tafel slope, and long-term stability for over 60 h without degradation toward oxygen evolution reaction in a 1.0 M KOH electrolyte. The Ni–Fe–O composite was used as the catalyst for both anode and cathode in an alkaline water electrolyzer. This electrolyzer demonstrated an excellent electrolysis performance and a long-term durability. The nice performance is believed from the unique mesoporous nanowire network architecture and the synergistic effect of the metal core and the active metal oxide. These provided the high active surface area and allowed the accelerated electron/ion transport for the fast electrolysis to generate hydrogen.

Cuprous oxide (Cu_2O) as a p-type semiconductor possesses the light absorption band falling into the visible light spectrum. Its direct band gap is 2.17 eV, which makes it suitable to be used as a hole-generation layer for photovoltaics. Dan et al. [122] prepared two types of cupric oxide (Cu_2O) nanoarchitectures (nanobelts and nanopetal networks) by immersing nanoporous copper (NPC) templates in anhydrous ethanol. The NPC templates with different defect densities were made by dealloying amorphous $Ti_{60}Cu_{40}$ ribbons in a mixture solution of hydrofluoric acid and polyvinylpyrrolidone (PVP) with different ratios of HF/PVP. Water molecule acted as the OH^- reservoir and the ethanol molecule served as a stabilizing or capping reagent for inhibiting the random growth of Cu_2O. Thus, the formation of 2-dimensional Cu_2O nanoarchitectures as shown in Figure 11 was observed. Figure 11a illustrates the small sized nanobelt in the Cu_2O layer, while Figure 11b reveals large sized nanosheets covering the nanobelts. The nanobelts are preferred to form in anhydrous ethanol on the NPC templates from $Ti_{60}Cu_{40}$ ribbons dealloyed in the solution with low HF concentration and small addition of PVP. The Cu_2O nanopetals grow in anhydrous ethanol on the NPC templates which were made from $Ti_{60}Cu_{40}$ ribbons dealloyed in the solution with high HF concentration and large addition of PVP. With increasing the immersion time in anhydrous ethanol, Cu_2O nanopetals aggregated together to form porous networks about 300 nm in thickness. The defect sites (i.e., twin boundary) on the nanoporous Cu ligaments served as the nucleation sites for Cu_2O nanocrystals. The higher the defect density, the more uniform the Cu_2O layer. A synergistic effect of the initial microstructure of NPC templates and the stabilizing agent of ethanol molecule resulted in different morphological features of the nanoporous Cu_2O [122].

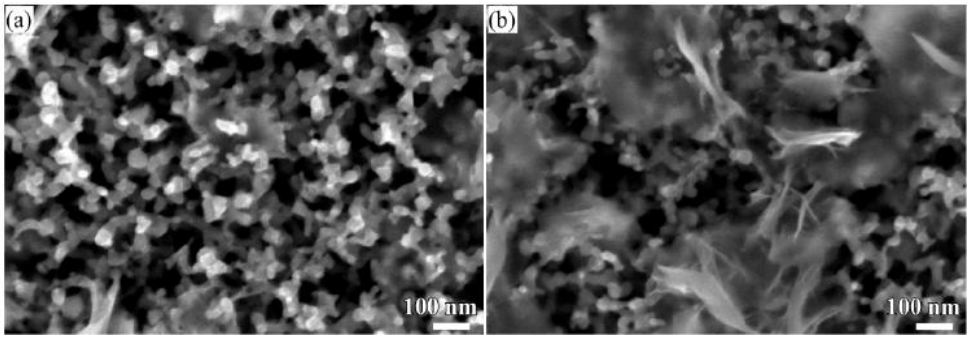

Figure 11. SEM images of porous Cu_2O nanoporous layer made by dealloying $Ti_{60}Cu_{40}$ ribbon in 0.65 M HF + 0.1 M PVP solution followed by immersion in anhydrous ethanol for 5 h: (a) small nanobelts, (b) large nanosheets [122]. Reprinted (adapted) with permission from Ref. [122].

5.3. Sensing and actuating

It is important to design and fabricate nanoporous metals (NPMs) with optimized microstructures for sensing and actuating applications. In [123], a hierarchical nanoporous gold (HNPG) membrane with a bimodal pore size distribution was prepared by dealloying $Au_{35}Ag_{65}$ in concentrated nitric acid first. Then the dealloyed sample was treated with 1 wt% H_3BO_3. The HNPG exhibits a wide pore distribution from 10 to 120 nm. The special architecture of HNPG significantly enhances the Raman signal to crystal violet and electrocatalytic activity toward the oxidation of methanol. The formation mechanism of the bimodal structure is discussed. It is proposed that the dehydration of H_3BO_3 can deposit HBO_2 or B_2O_3 on the walls of the Au ligaments. The surface diffusion of Au atom is inhibited. Correspondingly, the activation energy, Q, increases, resulting in the formation of lower hierarchy channels during the rearrangement of Au atoms.

Nanoporous coppers (NPCs) with controllable thicknesses and pore sizes were fabricated via the combination of a co-sputtering of Cu/Ti with a subsequent dealloying process. The effect of dealloying time on the porous morphology and the corresponding surface enhanced Raman scattering (SERS) behavior were systematically investigated. Transmission electron microscopy (TEM) identified the presences of the gaps formed between ligaments and also the nanobumps on the nanoparticle-aggregated ligament surface, which were likely to contribute as the "hot spots" for electromagnetic enhancement. The optimal NPC film exhibited excellent SERS performance towards sensing the Rhodamine 6G (R6G) with a low limiting detection of 10^{-9} M, along with good uniformity and reproducibility. The calculated enhancement factor of ca. 4.71×10^7 was over Au substrates and comparable to Ag systems, suggesting the proposed NPC as a candidate for high-performance SERS based sensing and detection [124].

Nanoporous gold nanoparticles (NPG-NPs) with controlled particle size and pore size possess high tenability of the plasmonic resonances, which is useful for sensing biological species. Rao et al. [125] fabricated nanoporous gold nanoparticles using a combination of solid-state dewetting and a subsequent dealloying process. Because of the combined effects of size and porosity, the NPG-NPs exhibit greater plasmonic tunability and significantly higher local field enhancement as compared to solid NPs. The effects of the nanoscale porosity and pore size on the optical extinction were investigated for the NPG-NPs with different particle sizes experimentally and theoretically. The influences of both porosity and pore size on the plasmonic properties are very complicated and clearly different for small particles with dominated dipole mode and large particles with dominated quadrupole mode. Au/Al_2O_3 hybrid porous NPs with controlled porosity and composition ratio were fabricated through plasma-enhanced atomic layer deposition of Al_2O_3 into the porous structure. In the Au/Al_2O_3 hybrid porous NPs, both Au and Al_2O_3 components were bicontinuously percolated over the entire structure. A further redshift of the plasmon peak was observed in the hybrid NPs due to the change of the environmental refractive index. The high tunability of the plasmonic resonances in the NPG-NPs and the hybrid porous NPs can be very useful for many applications in sensing biological and organic molecules.

Nanoporous copper has been proposed to be used as a glucose sensing material [126]. The freestanding hierarchical nested-network porous copper (HNNPC) was made by one-step free dealloying. The $Al_{75}Cu_{25}$ precursor alloy was prepared with both pure Al phase and the intermetallic Al_2Cu phase. The microstructure of the alloy led to the hierarchical porous structure characterized by larger ligaments (pores) at micron scale (3–4 μm) and the smaller ligaments (pores) at nanoscale

(50–60 nm) through dealloying. The morphology, crystal structure, elemental analysis, surface area, pore sizes distribution, electrochemical and sensing properties of the HNNPC have been studied. The resulted HNNPC had bicontinuous hierarchical structure, which met the electrochemical or chemical application requirements, i.e., the larger pores providing rapid transport pathways for fast switching and the smaller pores at nanoscale having the large surface area for functionalization. The HNNPC showed a high sensitivity to glucose.

A chemiresistive sensor based on porous SnO_2 was made through dealloying followed by thermal annealing [127]. The humidity sensing test at room temperature showed a high sensitivity of 348 in a fully humid atmosphere with an accuracy of 1% RH change. The sensor was found highly durable and reproducible. This sensor was also tested for electronic listening toward speaking, whistling, and breath monitoring. The results revealed the applicability of the resistive humidity sensor for electronic listening and biomedical sensing.

The surface enhanced Raman scattering (SERS) capability of the as-prepared nanoporous gold was evaluated using 4,4'-bi-pyridine as the probe molecule [128]. The $Au_{30}Cu_{35}Ag_7Pd_3Si_{20}$ amorphous alloy was chemically de-alloyed in acid. A comparison between samples dealloyed in nitric acid with and without HF was conducted to achieve homogeneous dealloying. The morphology and structure of the nanoporous gold (NPG) were adjusted by tuning the dealloying parameters, such as HNO_3 concentration, electrolyte temperature and dealloying time.

In addition to the sensing applications, dealloyed nanoporous metals have been considered to build actuators. Actuation of a hybrid nanomaterial was demonstrated by electro-polymerizing pyrrole on the internal surfaces of a dealloying-derived nanoporous gold [129]. The organic electrolyte was imbibed in the remaining pore space. The active polypyrrole films are contacted by two separate but individually contiguous conduction paths. This allowed efficient transport of ions in the electrolyte channels and of electrons in the gold ligaments. The ligaments also enhanced the mechanical behavior of the actuator. The actuation mechanism was based on the dimension changes of the polymer when ions were exchanged with the electrolyte in a pseudo-capacitive way, at potentials negative of the classic oxidation/reduction of polypyrrole. The experiments with millimeter-size bulk samples indicate fast switching and substantially larger strain amplitude than nanoporous metal actuators.

Most of the traditional metallic actuators use noble metals. Recently, alloying of noble element with earth-abundant metal has been considered to lower the cost of actuation materials while keeping a significant strain response [130]. The design and fabrication of a bulk nanoporous nickel–palladium alloy by dealloying was conducted. The alloy with a hierarchically porous structure showed different actuation behavior in different electrolytes. The actuation responses are dependent on the adsorption–desorption of hydrogen/hydroxyl. The nature (clean or oxide-cover) of the ligament surface also affects the actuation behavior. The maximum reversible strain of the nickel–palladium actuator could reach 0.47% in potassium hydroxide solution, which is more powerful as compared with other metallic actuation materials.

5.4. Implants and other biological applications

Among various implant materials, porous magnesium has the closest density of bone. Besides that, magnesium and its alloys are biocompatible and biodegradable. Thus, magnesium has been recognized as one of the most promising implant materials. However, the fast electrochemical

corrosion of Mg deteriorates its mechanical integrity. In reference [131], a porous ZrO_2 ceramic layer was coated onto the surface of AZ31B magnesium alloy to form a ZrO_2–AZ31B composite. This improves the corrosion resistance of the Mg alloy significantly. The corrosion resistance of the coating was evaluated in simulated body fluid solution by electrochemical techniques. Higher open circuit potential, impedance and polarization resistance of ZrO_2–AZ31B indicate a higher corrosion resistance than that of the AZ31B substrate in simulated body fluid solution. The results suggest that fabricating a ZrO_2 ceramic coating on magnesium alloys is an effective method to decrease the degradation rate of magnesium alloys thereby better matching clinical requirements. Surface-porous Mg–Al alloys with different microstructures can be processed by electrochemical dealloying in a 0.6 M NaCl neutral solution [132]. A bimodal porous structure with 48 μm large pores and 266 nm honeycomb-like fine pores was obtained by direct electrochemical dealloying of as-cast $Mg_{80}Al_{20}$ alloy. Following annealing, the eutectic structure disappeared and a bicontinuous, single-sized, porous structure with 7 μm ligaments was created by an annealing-electrochemical dealloying approach. The pore formation mechanism is governed by selective dissolution of the alpha-Mg phase, which leaves the $Mg_{17}Al_{12}$ phase as the porous layer framework. Nanoporous metals obtained by dealloying have been studied for other biological applications. Recently there is a surge in the use of the porous metals for bioanalytical and biomedical applications. Examples include biosensors for detecting biomarkers of disease and multifunctional neural interfaces for monitoring and modulating the activity of neural tissues [133].

5.5. Signal recording

Electro-co-deposition of Au–Pt–Cu alloy nanoparticles combined with chemical dealloying Cu was reported as a convenient way for increasing the effective surface area of microelectrode sites, which could reduce electrode impedance and improve the quality of *in vivo* spike signal recording [134]. In order to reduce the impedance and improve *in vivo* neural recording performance of microelectrodes, rough-surfaced Au–Pt alloy nanoparticles with nanoporosity were deposited on gold microelectrode sites through electro-co-deposition of Au–Pt–Cu alloy nanoparticles, followed by chemical dealloying Cu. The prepared Au–Pt alloy nanoparticles exhibited cauliflower-like shapes and possessed very rough surfaces with many different sizes of pores. Characterization of the Au–Pt alloy nanoparticles modified gold microelectrode sites indicated that average impedance of rough-surfaced Au–Pt alloy nanoparticle-modified sites was only 4.7% of that of the bare gold microelectrode sites. The corresponding *in vitro* background noise in the range from 1 to 7500 Hz decreased to only one fifth of the bare gold microelectrode sites. Spontaneous spike signal recording was used to evaluate *in vivo* neural recording performance of the modified microelectrode sites. The results showed that the rough-surfaced Au–Pt alloy nanoparticle-modified microelectrode sites exhibited higher average spike signal-to-noise ratio (SNR) of 4.8 due to lower background noise compared to control microelectrodes.

5.6. Environment cleaning and pollution control

Dealloyed porous metals are proposed for carbon dioxide capture. Recently, the permeation performance of a silver-carbonate dual-phase CO_2 separation membrane with the porous silver matrix prepared by electrochemical dealloying method was reported [135]. The membrane showed

excellent CO_2/O_2 flux densities and stability over 500 h with a very low leakage rate. A new transport mechanism involving the change of dominant reactive sites from triple phase boundaries to two-phase boundaries is also proposed to understand behaviors of the membrane exhibited during the CO_2/O_2 permeation process. In [136], an electrochemistry-based mixed electron and carbonate-ion conducting metal–carbonate composite membrane with porous metal matrix was fabricated by a chemical dealloying method. The porous material exhibits superior CO_2/O_2 flux density and stability over a 900 h testing period. The results also demonstrate that the presence of H_2 in the sweeping gas can significantly enhance the CO_2 flux density as a result of increased gradient of chemical potential of oxygen and produce a pure stream of CO_2 and H_2O for easy downstream conversion. The fundamental mechanisms leading to the superior performance are also discussed. Noble-metal nanostructures are crucial for highly active materials in applications such as fuel cells, sensors, electrodes and catalysts. But they are expensive. A new and efficient method for the in-situ synthesis of platinum–nickel nanostructures on porous zirconia was reported [137]. Ni–Zr–Y metallic alloys with defined Zr/Y-ratios and small amounts of platinum were internally oxidized. An interpenetrating network of yttria-stabilized zirconia (YSZ) in pure nickel was formed. Dealloying of the nickel matrix generated a multimodal porous ceramic supported structure with platinum–nickel nanostructures on the surface of the zirconia. This network porous metal-ceramic has a broad spectrum for tailored functionality, for example in after-treatment of exhaust gases.

One of the effective carbon dioxide sequestration methods is through the dry reforming reaction shown as follows:

$$CH_4 + CO_2 \rightarrow 2CO + 2H_2 \uparrow \quad (11)$$

It is meaningful to harness greenhouse gas (CO_2) and shale gas (CH_4) because both are the sources for generating global warming. To make the reaction in Eq 11 with high efficiency, a nanoporous Ni–Co alloy was proposed [98]. The nanoporous NiCo was fabricated by dealloying. The in-situ transmission electron microscopic observation and local chemical analysis indicated that the dry reforming induced chemical demixing of Ni and Co accompanied by grain refinement led to synergic effects that increased the reaction rate.

CO and NO are poison gases. The reduction of these gases is necessary for cleaning the environment. It has been shown that a copper based nanoporous alloy is effective on oxidation of CO and reduction of NO [98]. The nanoporous CuNiMnO used was made by dealloying of Mn from a CuNiMn precursor alloy [138]. The resulting material was durable and active toward both NO reduction and CO oxidation at 400 ℃. It was tested for 10 days and the thermal-resistant characteristic was observed. The nanostructure was activated by the CO oxidation and NO reduction reactions due to the tangled active metal and the thermally stable oxide networks in the dealloyed nanoporous material.

6. Future perspectives and conclusions

Dealloying technology for processing porous metals and alloys has been an active research field. Traditional chemical and electrochemical methods have been studied for new porous structure construction and novel application exploration. The physical vacuum dealloying technique and the high temperature selective dissolution method have caught much attention because they possess simplicity and they are friendly to environment. Many important characteristics of the dealloyed

metals such as mechanical stability, surface activity, transport of charge and heat have been studied for novel applications especially in energy manufacturing and environment protection. Structure design is another aspect of advances in dealloying. The design of hierarchical micro- and nano-architectures is an important way for obtaining large surface areas while keeping the structural integrity of porous materials. Future directions may include the fundamental study of pore formation kinetics and the scalable manufacturing of dealloyed porous materials in large size and high throughput. The device and system integration for practical applications is another important field of research in the future.

Acknowledgements

This work is supported by the California State Polytechnic University Pomona 2018–2019 Provost Teacher-Scholar Program. We acknowledge all the authors who originally created the figures cited in this review paper.

Conflict of interest

The authors declare no conflict of interest.

References

1. Juarez T, Biener J, Weissmuller J, et al. (2017) Nanoporous metals with structural hierarchy: A review. *Adv Eng Mater* 19: 1700389.
2. Li D, Liao HY, Kikuchi H, et al. (2017) Microporous Co@C nanoparticles prepared by dealloying CoAl@C precursors: Achieving strong wideband microwave absorption via controlling carbon shell thickness. *ACS Appl Mater Inter* 9: 44704–44714.
3. Liu T, Pang Y, Zhu M, et al. (2014) Microporous Co@CoO nanoparticles with superior microwave absorption properties. *Nanoscale* 6: 2447–2454.
4. Chen Q, Ding Y, Chen MW (2018) Nanoporous metal by dealloying for electrochemical energy conversion and storage. *MRS Bull* 43: 43–48.
5. Jin HJ, Weissmüller J, Farkas D (2018) Mechanical response of nanoporous metals: A story of size, surface stress, and severed struts. *MRS Bull* 43: 35–42.
6. Kunduraci M (2016) Dealloying technique in the synthesis of lithium-ion battery anode materials. *J Solid State Electr* 20: 2105–2111.
7. Zhao CH, Wada T, De Andrade V, et al. (2018) Imaging of 3D morphological evolution of nanoporous silicon anode in lithium ion battery by X-ray nano-tomography. *Nano Energy* 52: 381–390.
8. Li H, Fang X, Li G, et al. (2018) Investigation on fabrication and capillary performance of multi-scale composite porous wick made by alloying-dealloying method. *Int J Heat Mass Tran* 127: 145–153.
9. Su L, Gan YX (2012) Nanoporous Ag and Ag–Sn anodes for energy conversion in photochemical fuel cells. *Nano Energy* 1: 159–163.
10. Inkrott DK, Willingham RL, Balster T, et al. (2011) Preparation and electrochemical catalytic property of Au–Ni alloy with porous structure. *J Alloy Compd* 509: l47–l51.

11. Zhang FM, Wang LL, Li P, et al. (2017) Preparation of nano to submicro-porous TiMo foams by spark plasma sintering. *Adv Eng Mater* 19: 1600600.
12. Heiden M, Huang S, Nauman E, et al. (2016) Nanoporous metals for biodegradable implants: Initial bone mesenchymal stem cell adhesion and degradation behavior. *J Biomed Mater Res A* 104: 1747–1758.
13. Ren YB, Li J, Yang K (2017) Preliminary study on porous high-manganese 316L stainless steel through physical vacuum dealloying. *Acta Metall Sin-Engl* 30: 731–734.
14. Morrish R, Dorame K, Muscat AJ (2011) Formation of nanoporous Au by dealloying AuCu thin films in HNO_3. *Scripta Mater* 64: 856–859.
15. Zhang XL, Li GJ, Duan D, et al. (2018) Formation and control of nanoporous Pt ribbons by two-step dealloying for methanol electro-oxidation. *Corros Sci* 135: 57–66.
16. Wang JY, Yang S (2018) Nanoporous copper fabricated by dealloying Mn–Cu precursors with minor nickel element addition and heat treatment coarsening. *Nano* 13: 1850058.
17. Liu H, Wang XL, Wang JX, et al. (2017) High electrochemical performance of nanoporous Fe_3O_4/CuO/Cu composites synthesized by dealloying Al–Cu–Fe quasicrystal. *J Alloy Compd* 729: 360–369.
18. Hao Q, Ye JJ, Xu CX (2017) Facile fabrication of Fe_3O_4 octahedra with bimodal conductive network of nanoporous Cu and graphene nanosheets for high-performance anode in Li-ion batteries. *J Alloy Compd* 727: 34–42.
19. Chauvin A, Heu WTC, Tessier PY, et al. (2016) Impact of the morphology and composition on the dealloying process of co-sputtered silver–aluminum alloy thin films. *Phys Status Solidi B* 253: 2167–2174.
20. Sun Y, Balk TJ (2008) A multi-step dealloying method to produce nanoporous gold with no volume change and minimal cracking. *Scripta Mater* 58: 727–730.
21. Maruya K, Yamauchi R, Narushima T, et al. (2013) Structure consideration of platinum nanoparticles constructing nanostructures obtained by electrochemical dealloying of a Cu–Pt alloy. *J Nanosci Nanotechno* 13: 2999–3003.
22. Wang S, Chen B, Liang YF, et al. (2018) A feasible strategy for fabricating surface porous network in Fe–Si ribbons. *Materials* 11: 701.
23. Paschalidou EM, Fiore G, Xue Y, et al. (2018) Comparing selective corrosion of Au-based amorphous, partially amorphous, and devitrified alloys. *J Alloy Compd* 745: 212–216.
24. Yang F, Li YG, Wei YH, et al. (2018) Electrochemical synthesis of a surface-porous $Mg_{70.5}Al_{29.5}$ eutectic alloy in a neutral aqueous NaCl solution. *Appl Surf Sci* 435: 1246–1248.
25. McCue I, Karma A, Erlebacher J (2018) Pattern formation during electrochemical and liquid metal dealloying. *MRS Bull* 43: 27–34.
26. Okulov IV, Okulov AV, Soldatov IV, et al. (2018) Open porous dealloying-based biomaterials as a novel biomaterial platform. *Mat Sci Eng C-Mater* 88: 95–103.
27. Mokhtari M, Le Bourlot C, Adrien J, et al. (2017) Cold-rolling influence on microstructure and mechanical properties of NiCr–Ag composites and porous NiCr obtained by liquid metal dealloying. *J Alloy Compd* 707: 251–256.
28. Adamek G (2017) Tantalum foams prepared by the thermal dealloying process. *Int J Refract Met H* 65: 88–93.
29. Wada T, Yubuta K, Kato H (2016) Evolution of a bicontinuous nanostructure via a solid-state interfacial dealloying reaction. *Scripta Mater* 118: 33–36.

30. Panagiotopoulos NT, Jorge AM, Rebai I, et al. (2016) Nanoporous titanium obtained from a spinodally decomposed Ti alloy. *Micropor Mesopor Mat* 222: 23–26.
31. Okulov IV, Okulov AV, Volegov AS, et al. (2018) Tuning microstructure and mechanical properties of open porous TiNb and TiFe alloys by optimization of dealloying parameters. *Scripta Mater* 154: 68–72.
32. Wada T, Geslin PA, Kato H (2018) Preparation of hierarchical porous metals by two-step liquid metal dealloying. *Scripta Mater* 142: 101–105.
33. Zhao CH, Wada T, De Andrade V, et al. (2017) Three-dimensional morphological and chemical evolution of nanoporous stainless steel by liquid metal dealloying. *ACS Appl Mater Inter* 9: 34172–34184.
34. Ren YB, Sun YX, Yang K (2016) Study on micron porous copper prepared by physical vacuum dealloying. *Acta Metall Sin-Engl* 29: 1144–1147.
35. Sun YX, Ren YB (2015) New preparation method of porous copper powder through vacuum dealloying. *Vacuum* 122: 215–217.
36. Sun YX, Ren YB, Yang K (2016) New preparation method of micron porous copper through physical vacuum dealloying of Cu–Zn alloys. *Mater Lett* 165: 1–4.
37. Zhang T, Sun YQ, Hang LF, et al. (2018) Periodic porous alloyed Au–Ag nanosphere arrays and their highly sensitive SERS performance with good reproducibility and high density of hotspots. *ACS Appl Mater Inter* 10: 9792–9801.
38. Yi Y, Zheng XY, Fu ZB, et al. (2018) Multi-scale modeling for predicting the stiffness and strength of hollow-structured metal foams with structural hierarchy. *Materials* 11: 380.
39. Li Q, Lian LX, Liu Y, et al. (2017) Synthesis, microstructure, and catalytic performance of monolithic low-density porous Au. *Adv Eng Mater* 19: 1700045.
40. Chauvin A, Stephant N, Du K, et al. (2017) Large-scale fabrication of porous gold nanowires via laser interference lithography and dealloying of gold–silver nano-alloys. *Micromachines* 8: 168.
41. Luc W, Jiao F (2016) Synthesis of nanoporous metals, oxides, carbides, and sulfides: beyond nanocasting. *Accounts Chem Res* 49: 1351–1358.
42. Zhang K, Tan X, Zhang J, et al. (2014) Template-dealloying synthesis of ultralow density Au foams with bimodal porous structure. *RSC Adv* 4: 7196–7201.
43. Zhang K, Tan X, Wu W, et al. (2013) Template synthesis of low-density gold foams: Density, microstructure and compressive strength. *Mater Res Bull* 48: 3499–3504.
44. Lee GH, An S, Jang SW, et al. (2017) Fabrication of nanoporous noble metal thin films by O_2 plasma dealloying. *Thin Solid Films* 631: 147–151.
45. Du HH, Zhou C, Xie XB, et al. (2017) Pseudocapacitance of nanoporous Ni@NiO nanoparticles on Ni foam substrate: Influence of the annealing temperature. *Int J Hydrogen Energ* 42: 15236–15245.
46. Pang Y, Xie XB, Li D, et al. (2017) Microporous Ni@NiO nanoparticles prepared by chemically dealloying Al_3Ni_2@Al nanoparticles as a high microwave absorption material. *J Magn Magn Mater* 426: 211–216.
47. Li H, Zhu M, Pang Y, et al. (2016) Influences of ultrasonic irradiation on the morphology and structure of nanoporous Co nanoparticles during chemical dealloying. *Prog Nat Sci-Mater* 26: 562–566.

48. Zhang HX, Wang ZF, Yang MZ, et al. (2017) The effect of an external magnetic field on the dealloying process of the Ni–Al alloy in alkaline solution. *Phys Chem Chem Phys* 19: 18167–18171.
49. Tsurusawa H, Russo J, Leocmach M, et al. (2017) Formation of porous crystals via viscoelastic phase separation. *Nat Mater* 16: 1022–1023.
50. Lu Y, Ye WC, Yang Q, et al. (2016) Three-dimensional hierarchical porous PtCu dendrites: A highly efficient peroxidase nanozyme for colorimetric detection of H_2O_2. *Sensor Actuat B-Chem* 230: 721–730.
51. Ye W, Chen Y, Zhou F, et al. (2012) Fluoride-assisted galvanic replacement synthesis of Ag and Au dendrites on aluminum foil with enhanced SERS and catalytic activities. *J Mater Chem* 22: 18327–18334.
52. Barman BK, Nanda KK (2015) Uninterrupted galvanic reaction for scalable and rapid synthesis of metallic and bimetallic sponges/dendrites as efficient catalysts for 4-nitrophenol reduction. *Dalton T* 44: 4215–4222.
53. Liu J, Wu Q, Huang F, et al. (2013) Facile preparation of a variety of bimetallic dendrites with high catalytic activity by two simultaneous replacement reactions. *RSC Adv* 3: 14312–14321.
54. Esque-de los Ojos D, Zhang J, Fornell J, et al. (2016) Nanomechanical behaviour of open-cell nanoporous metals: Homogeneous versus thickness-dependent porosity. *Mech Mater* 100: 167–174.
55. Farghaly AA, Khan RK, Collinson MM (2018) Biofouling-resistant platinum bimetallic alloys. *ACS Appl Mater Inter* 10: 21103–21112.
56. Frei M, Kohler C, Dietel L, et al. (2018) Pulsed electrodeposition of highly porous Pt alloys for use in methanol, formic acid, and glucose fuel cells. *ChemElectroChem* 5: 1013–1023.
57. Lin JD, Chou CT (2017) The influence of acid etching on the electrochemical supercapacitive properties of Ni–P coatings. *Surf Coat Tech* 325: 360–369.
58. Lilleodden ET, Voorhees PW (2018) On the topological, morphological, and microstructural characterization of nanoporous metals. *MRS Bull* 43: 20–26.
59. Song T, Yan M, Qian M (2018) The enabling role of dealloying in the creation of specific hierarchical porous metal structures—A review. *Corros Sci* 134: 78–98.
60. Liu WB, Cheng P, Yan JZ, et al. (2018) Temperature-induced surface reconstruction and interface structure evolution on ligament of nanoporous copper. *Sci Rep* 8: 447.
61. Wang ZL, Ning SC, Liu P, et al. (2017) Tuning surface structure of 3D nanoporous gold by surfactant-free electrochemical potential cycling. *Adv Mater* 29: 1703601.
62. Zhang JM, Ma F, Xu KW (2004) Calculation of the surface energy of FCC metals with modified embedded-atom method. *Appl Surf Sci* 229: 34–42.
63. Fujita T (2017) Hierarchical nanoporous metals as a path toward the ultimate three-dimensional functionality. *Sci Technol Adv Mat* 18: 724–740.
64. Lian LX, Yao YF, Liu Y, et al. (2017) A segmental dealloying for fabricating the gradient nanoporous metal materials. *J Porous Mat* 24: 211–215.
65. Pia G, Cincotti A, Delogu F (2016) Thermally and catalytically induced coarsening of nanoporous Au. *Mater Lett* 183: 114–116.
66. Schubert I, Huck C, Krober P, et al. (2016) Porous gold nanowires: Plasmonic response and surface-enhanced infrared absorption. *Adv Opt Mater* 4: 1838–1845.

67. Serin RB, Abdullayeva N, Sankir M (2017) Dealloyed ruthenium film catalysts for hydrogen generation from chemical hydrides. *Materials* 10: 738.
68. Chauvin A, Delacote C, Boujtita M, et al. (2016) Dealloying of gold–copper alloy nanowires: From hillocks to ring-shaped nanopores. *Beilstein J Nanotech* 7: 1361–1367.
69. Gao JJ, Qiu HJ, Wen YR, et al. (2016) Enhanced electrochemical supercapacitance of binder-free nanoporous ternary metal oxides/metal electrode. *J Colloid Interf Sci* 474: 18–24.
70. Zhang X, Hashimoto T, Lindsay J, et al. (2016) Investigation of the de-alloying behaviour of theta-phase (Al_2Cu) in AA2024-T351 aluminium alloy. *Corros Sci* 108: 85–93.
71. Ruestes CJ, Schwen D, Millan EN, et al. (2018) Mechanical properties of Au foams under nanoindentation. *Comp Mater Sci* 147: 154–167.
72. Wang CY, Li M, Zhu M, et al. (2017) Controlling the mechanical properties of bulk metallic glasses by superficial dealloyed layer. *Nanomaterials* 7: 352.
73. Qin CL, Wang CY, Hu QF, et al. (2016) Hierarchical nanoporous metal/BMG composite rods with excellent mechanical properties. *Intermetallics* 77: 1–5.
74. Liu F, Ye XL, Jin HJ (2017) Anomalous low strain induced by surface charge in nanoporous gold with low relative density. *Phys Chem Chem Phys* 19: 19217–19224.
75. Ngo BND, Roschning B, Albe K, et al. (2017) On the origin of the anomalous compliance of dealloying-derived nanoporous gold. *Scripta Mater* 130: 74–77.
76. Cao YK, Ma XY, Chen YZ, et al. (2016) Size effect of ligaments on charge induced surface stress response of nanoporous Pd prepared by dealloying. *Scripta Mater* 123: 1–4.
77. Weissmüller J, Cahn JW (1997) Mean stresses in microstructures due to interface stresses: A generalization of a capillary equation for solids. *Acta Mater* 45: 1899–1906.
78. Viswanath RN, Kramer D, Weismüller J (2005) Variation of the surface stress–charge coefficient of platinum with electrolyte concentration. *Langmuir* 21: 4604–4609.
79. Viswanath RN, Kramer D, Weismüller J (2008) Adsorbate effects on the surface stress–charge response of platinum electrodes. *Electrochim Acta* 53: 2757–2767.
80. Viswanath RN, Weismüller J (2013) Electrocapillary coupling coefficients for hydrogen electrosorption on palladium. *Acta Mater* 61: 6301–6309.
81. Ye XL, Jin HJ (2016) Corrosion-induced strengthening: Development of high-strength nanoporous metals. *Adv Eng Mater* 18: 1050–1058.
82. Kim NJ, Lin MS (2010) A nanoporous metallic mat showing excellent and stable surface enhanced Raman spectroscopy activities. *J Nanosci Nanotechno* 10: 5077–5082.
83. Zeng Y, Zhang J, Dong X, et al. (2014) Pd based nanoporous metals with superior catalytic activity. *Mater Res Innov* 18: S4-734–S4-739.
84. Wang SS, Zhang C, Li HY, et al. (2017) Enhanced electro-catalytic performance of Pd-based amorphous nanoporous structure synthesized by dealloying $Pd_{32}Ni_{48}P_{20}$ metallic glass. *Intermetallics* 87: 6–12.
85. Weissmuller J, Sieradzki K (2018) Dealloyed nanoporous materials with interface-controlled behavior. *MRS Bull* 43: 14–19.
86. Zhou M, Huang X, Hagos K, et al. (2017) Nanoporous copper fabricated from $Zr_{65}Cu_{17.5}Fe_{10}Al_{7.5}$ amorphous alloy and its electrocatalytic oxidation performance. *Intermetallics* 90: 23–29.
87. Wang ZF, Fei PY, Xiong HQ, et al. (2017) $CoFe_2O_4$ nanoplates synthesized by dealloying method as high performance Li-ion battery anodes. *Electrochim Acta* 252: 295–305.

88. Okulov AV, Volegov AS, Weissmuller J, et al. (2018) Dealloying-based metal-polymer composites for biomedical applications. *Scripta Mater* 146: 290–294.
89. Wang Y, Huang W, Si CH, et al. (2016) Self-supporting nanoporous gold–palladium overlayer bifunctional catalysts toward oxygen reduction and evolution reactions. *Nano Res* 9: 3781–3794.
90. Song YY, Zhang XL, Yang S, et al. (2016) Electrocatalytic performance for methanol oxidation on nanoporous Pd/NiO composites prepared by one-step dealloying. *Fuel* 181: 269–276.
91. Li X, Qiu HJ, Wang JQ, et al. (2016) Corrosion of ternary Mn–Cu–Au to nanoporous Au–Cu with widely tuned Au/Cu ratio for electrocatalyst. *Corros Sci* 106: 55–60.
92. Giarratano F, Arzac GM, Godinho V, et al. (2018) Nanoporous Pt-based catalysts prepared by chemical dealloying of magnetron-sputtered Pt–Cu thin films for the catalytic combustion of hydrogen. *Appl Catal B-Environ* 235: 168–176.
93. Qiu HJ, Gao JJ, Chiang FK, et al. (2018) A general and scalable approach to produce nanoporous alloy nanowires with rugged ligaments for enhanced electrocatalysis. *J Mater Chem A* 6: 12541–12550.
94. Zhang XL, Duan D, Li GJ, et al. (2018) Monolithic Au/CeO_2 nanorod framework catalyst prepared by dealloying for low-temperature CO oxidation. *Nanotechnology* 29: 095606.
95. Zhang WQ, He J, Liu SY, et al. (2018) Atomic origins of high electrochemical CO_2 reduction efficiency on nanoporous gold. *Nanoscale* 10: 8372–8376.
96. Zhou QX, Qi L, Yang HX, et al. (2018) Hierarchical nanoporous platinum–copper alloy nanoflowers as highly active catalysts for the hydrolytic dehydrogenation of ammonia borane. *J Colloid Surf Sci* 513: 258–265.
97. Kim YT, Lopes PP, Park SA, et al. (2017) Balancing activity, stability and conductivity of nanoporous core–shell iridium/iridium oxide oxygen evolution catalysts. *Nat Commun* 8: 1449.
98. Fujita T, Higuchi K, Yamamoto Y, et al. (2017) In-situ TEM study of a nanoporous Ni–Co catalyst used for the dry reforming of methane. *Metals* 7: 406.
99. Sarkar S, Subbarao U, Peter SC (2017) Evolution of dealloyed $PdBi_2$ nanoparticles as electrocatalysts with enhanced activity and remarkable durability in hydrogen evolution reactions. *J Mater Chem A* 5: 15950–15960.
100. Mahr C, Kundu P, Lackmann A, et al. (2017) Quantitative determination of residual silver distribution in nanoporous gold and its influence on structure and catalytic performance. *J Catal* 352: 52–58.
101. Xiao XX, Engelbrekt C, Zhang MW, et al. (2017) A straight forward approach to electrodeposit tungsten disulfide/poly(3,4-ethylenedioxythiophene) composites onto nanoporous gold for the hydrogen evolution reaction. *Appl Surf Sci* 410: 308–314.
102. Xu CX, Hao Q, Zhao DY (2016) Facile fabrication of a nanoporous Si/Cu composite and its application as a high-performance anode in lithium-ion batteries. *Nano Res* 9: 908–916.
103. Zhao H, Lei DN, He YB, et al. (2018) Compact 3D copper with uniform porous structure derived by electrochemical dealloying as dendrite-free lithium metal anode current collector. *Adv Energy Mater* 8: 1800266.
104. Fujita T (2017) Hierarchical nanoporous metals as a path toward the ultimate three-dimensional functionality. *Sci Technol Adv Mat* 18: 724–740.
105. Ding Y, Erlebacher J (2003) Nanoporous metals with controlled multimodal pore size distribution. *J Am Chem Soc* 125: 7772–7773.

106. Qi Z, Weissmüller J (2013) Hierarchical nested-network nanostructure by dealloying. *ACS Nano* 7: 5948–5954.
107. Qin H, Shamso AE, Centeno A, et al. (2017) Enhancement of the up conversion photoluminescence of hexagonal phase $NaYF_4$:Yb^{3+}, Er^{3+} nanoparticles by mesoporous gold films. *Phys Chem Chem Phys* 19: 19159–19167.
108. Wang L, Lu DF, Gao R, et al. (2017) Theoretical analyses and chemical sensing application of surface plasmon resonance effect of nanoporous gold films. *Acta Phys-Chim Sin* 33: 1223–1229.
109. Lin B, Kong LX, Hodgson PD, et al. (2017) Controlled porosity and pore size of nano-porous gold by thermally assisted chemical dealloying—a SAXS study. *RSC Adv* 7: 10821–10830.
110. Fratzl P, Weinkamer R (2007) Nature's hierarchical materials. *Prog Mater Sci* 52: 1263–1334.
111. Luhrs L, Weissmuller J (2018) Nanoporous copper-nickel—Macroscopic bodies of a strong and deformable nanoporous base metal by dealloying. *Scripta Mater* 155: 119–123.
112. Liu T, Pang Y, Xie XB, et al. (2016) Synthesis of microporous Ni/NiO nanoparticles with enhanced microwave absorption properties. *J Alloy Compd* 667: 287–296.
113. Sohn M, Lee DG, Park HI, et al. (2018) Microstructure controlled porous silicon particles as a high capacity lithium storage material via dual step pore engineering. *Adv Funct Mater* 28: 1800855.
114. Detsi E, Petrissans X, Yan Y, et al. (2018) Tuning ligament shape in dealloyed nanoporous tin and the impact of nanoscale morphology on its applications in Na-ion alloy battery anodes. *Phys Rev Mater* 2: 055404.
115. Gao H, Niu JZ, Zhang C, et al. (2018) A dealloying synthetic strategy for nanoporous bismuth-antimony anodes for sodium ion batteries. *ACS Nano* 12: 3568–3577.
116. Luo Z, Xu JC, Yuan B, et al. (2018) A novel 3D bimodal porous current collector with large interconnected spherical channels for improved capacity and cycling stability of Sn anode in Li-ion batteries. *Mater Lett* 213: 189–192.
117. Liu H, Wang XL, Wang JX, et al. (2017) Hierarchical porous CoNi/CoO/NiO composites derived from dealloyed quasicrystals as advanced anodes for lithium-ion batteries. *Scripta Mater* 139: 30–33.
118. Yang H, Qiu HJ, Wang JQ, et al. (2017) Nanoporous metal/metal-oxide composite prepared by one-step de-alloying AlNiCoYCu metallic glasses. *J Alloy Compd* 703: 461–465.
119. Guo XW, Han JH, Liu P, et al. (2016) Hierarchical nanoporosity enhanced reversible capacity of bicontinuous nanoporous metal based Li-O_2 battery. *Sci Rep* 6: 33466.
120. Yun QB, He YB, Lv W, et al. (2016) Chemical dealloying derived 3D porous current collector for Li metal anodes. *Adv Mater* 28: 6932–6939.
121. Dong CQ, Kou TY, Gao H, et al. (2018) Eutectic-derived mesoporous Ni–Fe–O nanowire network catalyzing oxygen evolution and overall water splitting. *Adv Energy Mater* 8: 1701347.
122. Dan ZH, Lu JF, Li F, et al. (2018) Ethanol-mediated 2D growth of Cu_2O nanoarchitectures on nanoporous Cu templates in anhydrous ethanol. *Nanomaterials* 8: 18.
123. Chen AY, Qiu YJ, Zhu YK, et al. (2016) Facile fabrication of nanoporous gold with bimodal pore structure. *Mater Lett* 184: 282–285.
124. Diao FY, Xiao XX, Luo B, et al. (2018) Two-step fabrication of nanoporous copper films with tunable morphology for SERS application. *Appl Surf Sci* 427: 1271–1279.
125. Rao W, Wang D, Kups T, et al. (2017) Nanoporous gold nanoparticles and Au/Al_2O_3 hybrid nanoparticles with large tunability of plasmonic properties. *ACS Appl Mater Inter* 9: 6273–6281.

126. Li XQ, Huang BS, Qiu CC, et al. (2016) Hierarchical nested-network porous copper fabricated by one-step dealloying for glucose sensing. *J Alloy Compd* 681: 109–114.
127. Solanki V, Krupanidhi SB, Nanda KK (2017) Sequential elemental dealloying approach for the fabrication of porous metal oxides and chemiresistive sensors thereof for electronic listening. *ACS Appl Mater Inter* 9: 41428–41434.
128. Xue YP, Scaglione F, Rizzi P, et al. (2017) Improving the chemical de-alloying of amorphous Au alloys. *Corros Sci* 127: 141–146.
129. Wang K, Stenner C, Weissmller J (2017) A nanoporous gold–polypyrrole hybrid nanomaterial for actuation. *Sensor Actuat B-Chem* 248: 622–629.
130. Zhang J, Lv LF, Gao H, et al. (2017) Electrochemical actuation behaviors and mechanisms of bulk nanoporous Ni–Pd alloy. *Scripta Mater* 137: 73–77.
131. Gao YE, Zhao LF, Yao XH, et al. (2018) Corrosion behavior of porous ZrO_2 ceramic coating on AZ31B magnesium alloy. *Surf Coat Tech* 349: 434–441.
132. Yang F, Yan ZY, Wei YH, et al. (2018) Fabrication of surface-porous Mg–Al alloys with different microstructures in a neutral aqueous solution. *Corros Sci* 130: 138–142.
133. Şeker E, Shih WC, Stine KJ (2018) Nanoporous metals by alloy corrosion: Bioanalytical and biomedical applications. *MRS Bull* 43: 49–56.
134. Zhao ZY, Gong RX, Zheng L, et al. (2016) *In vivo* neural recording and electrochemical performance of microelectrode arrays modified by rough-surfaced AuPt alloy nanoparticles with nanoporosity. *Sensors* 16: 1851.
135. Fang J, Xu NS, Yang TR, et al. (2017) CO_2 capture performance of silver-carbonate membrane with electrochemically dealloyed porous silver matrix. *J Membrane Sci* 523: 439–445.
136. Fang J, Tong JJ, Huang K (2016) A superior mixed electron and carbonate-ion conducting metal-carbonate composite membrane for advanced flue-gas carbon capture. *J Membrane Sci* 505: 225–230.
137. Terock M, Konrad CH, Popp R, et al. (2016) Tailored platinum-nickel nanostructures on zirconia developed by metal casting, internal oxidation and dealloying. *Corros Sci* 112: 246–254.
138. Fujita T, Abe H, Tanabe T, et al. (2016) Earth-abundant and durable nanoporous catalyst for exhaust-gas conversion. *Adv Funct Mater* 26: 1609–1616.

AIMS Press